

On universal features of the turbulent cascade and its non-equilibrium thermodynamic process

Nico Reinke^{1,2,4}, Daniel Nickelsen^{1,3}, and Joachim Peinke^{1,2}

¹ Institute of Physics, University of Oldenburg and

² ForWind, University of Oldenburg, Carl-von-Ossietzky-Str. 9-11, 26129 Oldenburg, Germany

³ National Institute for Theoretical Physics (NITheP), Stellenbosch 7600, South Africa

⁴ Corresponding author - Email: nicoreinke@gmx.de

December 13, 2024

Abstract

We analyse various turbulent flows based on their 2-point and multi-scale statistics. Datasets are measured in free jets and wake flows of a regular grid and a cylinder. 2-point statistics are characterised by structure functions of velocity increments. The multi-scale characterisation is based on the Markov property of the turbulent cascade, which allows to reduce the multi-scale process to the description of conditional probability density functions (cPDF) in scale, what corresponds to a three point closure. The evolution of cPDF in scale is described by the Fokker-Planck equation and its Kramers-Moyal coefficients (KMCs). KMCs are obtained by a self-consistent optimisation procedure, which is based on measured data. We show the validity of the integral fluctuations theorem (IFT) for all datasets, which is a law of non-equilibrium thermodynamics. It enables to show evidence for the explicit functional form of KMCs and supports that the structure functions get a closed functional form, given by the Fokker-Planck formalism, which contradicts to proper scaling of the structure functions. The combination of optimisation and IFT allows a valid comparison of 2-point and multi-scale analysis. In contrast, to the results of the 2-point analysis, we show that the multi-scale analysis separates the cascade process into universal and non-universal shares regarding the different turbulent flows. We conclude that stochastic analysis in terms of KMCs enables to unfold the specific generation mechanism of turbulence and its large scale motion.

1 Introduction

A general description of turbulent flows remains one of the most challenging unsolved scientific problems, e.g. Nelkin (1992); Clay (2000). Of particular importance is the simplified problem of homogenous isotropic turbulence (HIT). HIT is not only often the starting point for fundamental studies, but also important for applications like for CFD-modeling, where the features of small scale turbulence are essential for simplifications, e.g. Pope (2000).

One important question for the understanding of the turbulent cascade, cf. Richardson (1922), is how turbulent structures evolve within the inertial range from large to small scales. Strongly related to this issue is the question whether turbulent structures evolve in the cascade in a universal way or whether the evolution depends on the generation process and its specific large scale features. With other words, how long do large turbulent structures have a significant impact to small scale features. This central question is frequently discussed in literature since the contributions of Kolmogorov and Landau, cf. Frisch (2001, pp. 93-98) and is essential for the concept of the universal small scale turbulence.

The overwhelming majority of studies investigate turbulence by statistics of increments u_r like structure functions $S^K(u_r)$. For HIT scaling features for the structure functions as function of scale r are commonly assumed, characterised by scaling exponent ξ_K (Kolmogorov, 1941, 1962; Frisch, 2001; Davidson, 2004; Pope, 2000). Universality is assumed to be found in the scaling exponents ξ_K , whereas pre-factors may change with different flow conditions, cf. Kolmogorov (1962). Recent works, e.g. Kuczaj et al. (2006); Hurst and Vassilicos (2007); Valente and Vassilicos (2012); Nagata et al. (2013), are particular interested, in this context, in the understanding of multi-scale excited turbulent flows and its structures.

Note that the structure function analysis can be expressed equivalently by probability density functions $p(u_r)$ (PDF). From a statistical point of view, structure functions as well as increment PDFs are two point quantities, i.e. these investigate the relation of velocities at two points separated by a selected distance, the scale r .

It was shown (e.g. by Renner et al. (2001)) that 2-point statistics do not characterise completely the features of small scale turbulence. A general multi-scale characterisation of the turbulent cascade can be expressed by the joint probability $p(u_r; u_{r+\Delta}; \dots; u_{r+N\Delta})$ over N scales r . Since velocity increment series show the Markov property, the joint probability can equally be expressed by a chain of conditional PDFs $p(u_r|u_{r+\Delta})$, cf. Friedrich and Peinke (1997); Renner et al. (2001); Tutkun and Mydlarski (2004). Note, this Markov property corresponds to a two-scale or three-point closure of

the generalised multi-scale joint probability. Furthermore, the evolution of this transition probability $p(u_r|u_{r+\Delta})$ along the scale can be described by the Fokker-Planck equation, where only the Kramers-Moyal coefficients $D^{(1)}(u_r)$ and $D^{(2)}(u_r)$ govern the equation. Thus, the description of the turbulent cascade along the inertial range reduces to the determination of these two Kramers-Moyal coefficients. Thereby, different cascades, measured in different turbulent flows, can be set into a quantitative comparison with their stochastic process equations. Note, likewise to this approach, other approaches contain equivalent multi-scale information of the turbulent cascade cf. Lundgren (1967); Monin (1967); L'vov and Procaccia (1996); Davoudi and Tabar (2000); Monin et al. (2007).

Renner et al. (2001) investigated turbulent data generated in free jets with such a multi-scale method, for a similar work investigating also passive scalars, see Tutkun and Mydlarski (2004); Melius et al. (2014). In this work the features of a turbulent flow was analysed in terms of Kramers-Moyal coefficients from which the stochastic flow features could be reconstructed. Moreover, the Kramers-Moyal coefficients were related to structure functions. In Renner et al. (2002) it was shown that the multi-scale statistics of free jet generated turbulent cascades change with Taylor-Reynolds number (Re_λ) and the issue of universal features of small scale turbulence was discussed.

Based on multi-scale statistics Stresing et al. (2010) found a new turbulent class of fractal grid generated turbulence, which has different scaling features and multi-scale statistics, than *commonly* generated flows (cylinder wake and free jet). The work of Stresing and Peinke (2010); Keylock et al. (2015) gives first indications that the turbulent cascade and its Kramers-Moyal coefficients depend on the turbulence generation mechanism.

This contrasts with the universal features found on the basis of 2-point statistics. Therefore, we revive this analysis with 2-point and multi-scale statistics and want to study the question of universality more in detail and in a more general, as well as, more systematic way.

Although the multi-scale statistics will deliver more details of the complex structure of turbulence, for this method remains the problem of accuracy in determining the Kramers-Moyal coefficients, since one has to bridge the Einstein-Markov length for their estimation, cf. R. Friedrich and Peinke (1998); Renner et al. (2001); Lück et al. (2006). Two ways to overcome this technical difficulty have been worked out. Firstly, the Kramers-Moyal coefficients are estimated by an optimisation procedure. Thus, Kramers-Moyal coefficients *matches best* to the experimental found data, namely $p(u_r|u_{r+\Delta})$, cf. Nawroth et al. (2007); Kleinhans et al. (2005). A second independent way for determining the *accuracy* of the Kramers-Moyal coefficients is based on the integral fluctuation theorem (IFT), cf. Seifert (2005), which is a generalised entropy law for non-equilibrium thermodynamics. Recently, the validity of the IFT for the turbulent cascade process has been shown by Nickelsen and Engel (2013). Here we confirm the validity of this basic law for our entire dataset and we will use the IFT as a criterium for the accuracy of the estimated stochastic process equations, since Nickelsen and Engel (2013) stressed the particular sensitivity of the IFT measure on the right estimation of Kramers-Moyal coefficients. Furthermore, the IFT enables to decide which functional contributions to the Kramers-Moyal coefficients are significant (see also a first use of this procedure for data analysis from turbulence generated by a fractal grid Reinke et al. (2016)). The combination of the optimisation procedure and the IFT will in the end allow to compare the complexity of different turbulence measurements with respect to their universality.

In this paper we analysed the longitudinal velocity increment component of 61 datasets, mostly measured by hot-wires, where the turbulence was generated by regular grid, cylinder and free jet. Note, the entire dataset is always used in our analysis, no single datasets are sorted out for reasons of clarity. These datasets cover a Taylor-Reynolds number range of $28 \leq Re_\lambda \leq 996$.

This paper is organised as follows: In section 2 we give more information about the analysed datasets, section 3 reports about the used methods regarding structure functions, the IFT and the multi-scale analysis. In section 4 the results are presented as well as discussed on the background of universality and section 5 concludes the paper.

2 Data basis

The data basis used in this study consists of 61 single datasets, which correspond to seven subgroups, namely i) regular grid generated turbulence, with $28 \leq Re_\lambda \leq 153$, cf. Lück et al. (2006), ii) cylinder wake turbulence at $\frac{x}{D}=40$ with $261 \leq Re_\lambda \leq 894$, cf. Lück et al. (2006), iii) cylinder wake turbulence at various positions $\frac{x}{D}=50, 60, 70, 80, 90$ and 100 with $Re_\lambda \approx 261$, cf. Lück et al. (2006), iv) free jet generated turbulence in helium at $\frac{x}{D}=40$ with $208 \leq Re_\lambda \leq 996$, cf. Chanal et al. (2000), v) free jet turbulence in air at $\frac{x}{D}=40$, vi) free jet turbulence in air at $\frac{x}{D}=60$ and vii) free jet turbulence in air at $\frac{x}{D}=80$.

The free jet data in air cover the Taylor Reynolds number range of $166 \leq Re_\lambda \leq 865$. x denotes in all cases the downstream position, D the cylinder diameter or the jet nozzle diameter. The subgroups i), ii), v)-vii) are measured with a single hot-wire probe and contain longitudinal velocity component measurements. The subgroup iii) is measured with a X-wire probe, therefore these data contain the longitudinal and one transversal velocity component. The subgroup iv) flow is measured with a special micro structured hot-point probe, cf. Chanal et al. (2000). This measurement technic is similar to a single hot-wire probe.

In the following, results of the single subgroups are indicated by the following markers and notations in the legend: i) open squares, *Grids*; ii) open circles, *Cylinders*; iii) solid circles, greyscale indicates $\frac{x}{D}$, the darker the larger $\frac{x}{D}$, *Cylinders* (x/D); iv) open triangles, *Jets He*; v) solid triangles, *Jets 40D*; vi) open triangles, *Jets 60D* and vii) solid triangles, *Jets*

Dataset	Re_λ [-]	L [mm]	λ [mm]	l_{EM} [mm]	Θ [mm]	σ_v [m/s]	σ_Θ [m/s]
i) grid	153	25.0	2.61	5.22	6.57	0.845	0.637
iii) cylinder	894	25.2	3.35	6.70	9.78	3.94	2.40
iv) jet (2)	996	1.95	0.186	0.372	0.464	0.183	0.119
vii) jet (1)	166	62.5	5.84	11.7	15.7	0.382	0.278

Table 1: Exemplary datasets and their characteristics

80D. Open and solid triangles are differently rotated, thus, these can be distinguished.

Four exemplary datasets are used to highlight analysis results. These datasets are chosen either to be comparable in terms of Taylor-Reynolds number Re_λ (namely 153 and 166 or 894 and 996) or to be comparable in the kind of turbulence generation. Characteristic quantities of these datasets are summarised in table 1. The listed quantities are, longitudinal integral length L , Taylor micro scale length λ , a newly defined Kolmogorov length scale Θ , standard deviation of the velocity σ_v and a newly defined normalising standard deviation σ_Θ .

The procedure proposed by Aronson and Löfdahl (1993) is used for the estimation of λ . Note, results of λ match with findings in Lück et al. (2006) and Renner et al. (2001). L is estimated by integrating autocorrelation function, cf. Batchelor (1953), in case of a non-monotonous decrease of the autocorrelation function (until the first zero crossing) a procedure is used, which extrapolates the autocorrelation function by an exponential function, cf. Reinke et al. (2014). More information regarding this procedure can be found in the appendix A1. Results of L match with findings in Lück et al. (2006) and Renner et al. (2001). Note, also the ratio $\frac{L}{\lambda}$ as function of Re_λ is shown in the appendix A1, which shows the consistency of the used datasets. Θ and σ_Θ are defined in section 3.

3 Methods of analysis

3.1 Classical analysis

At first, datasets of velocity time series are transferred to spatial velocity series by the use of Taylor's hypothesis,

$$v(dx) \approx v(-\langle v(t) \rangle dt), \quad (1)$$

where v denotes the velocity component in main flow direction, x is the spatial component in main flow direction, t is time and $\langle \dots \rangle$ denotes the expectation value. The kind of recording velocity is taken into account by the minus sign in eq. (1). This hypothesis of frozen turbulence is commonly known as a good approximation for small velocity fluctuations $\frac{v'}{\langle v \rangle} \ll 1$, cf. Taylor (1938), or small turbulence intensities, i.e. smaller than 10-20%, cf. Murzyn and B elorgey (2005). This limit is fulfilled for almost all datasets. Further discussion of the validity can be found e.g. in Lin (1950); Lumley (1965); Pinton, J. F. and Labb e, R. (1994); Tong and Warhaft (1995); Gledzer (1997).

A standard quantity to analyse the scaling of turbulence is the velocity increment

$$u_r^* := v(x+r) - v(x), \quad (2)$$

which is the difference of velocities at two points separated by the distance r , therefore its statistics are referred as 2-point statistics. Note, the spacial distance r we call further on as *scale*. A common analysing quantity for turbulence is the so-called structure function of order κ ,

$$S^\kappa(r) = \langle (u_r^*)^\kappa \rangle. \quad (3)$$

Within the inertial range it is commonly proposed that for homogenous isotropic turbulence structure functions scale according to a power law (Kolmogorov, 1941)

$$S^\kappa(r) \propto r^{\xi_\kappa}. \quad (4)$$

Kolmogorov (1962) proposed a refined approach for the structure function exponent with the functional form of

$$\xi_\kappa = \frac{\kappa}{3} - \frac{\mu}{18} \kappa(\kappa - 3), \quad (5)$$

with the experimentally measured intermittency factor $\mu \approx 0.26$, e.g. Arneodo et al. (1996). Note, ξ_κ proposed by Kolmogorov is constant in r . From experimental data a local scaling exponent $\xi_\kappa(r)$ can be calculated by the log-log-derivative of structure functions, here, the central difference quotient is used

$$\xi_\kappa(r) = \lim_{\delta r \rightarrow 0} \frac{\ln(\langle (u_{r+\delta r}^*)^\kappa \rangle) - \ln(\langle (u_{r-\delta r}^*)^\kappa \rangle)}{\ln(r+\delta r) - \ln(r-\delta r)}. \quad (6)$$

Experimental results (as shown below) show that the range of constant scaling, as proposed by Kolmogorov, is rather small or even infinitesimal in case of finite Taylor based Reynolds number ($Re_\lambda \leq 1000$). This motivates to define a specific

scale Θ by $\xi_2(\Theta) = 0.696$, at which Kolmogorov's proposed scaling is located. Correspondingly a standard deviation, $\sigma_\Theta = \sqrt{\langle (u_{r=\Theta}^*)^2 \rangle}$ is defined. Here, we call Θ *Kolmogorov scaling length* or *deep turbulence scale*.

For the comparison of the statistics of u_r^* it is necessary that velocity increments get normalised in a proper way. On the one side, we follow the way proposed by Renner et al. (2001) where a norm based on second order structure function is used and on the other side we are inspired by the work of Mydlarski and Warhaft (1996) where features of the inertial range are investigated. Thus we select σ_Θ for the purpose of normalisation

$$u_r := \frac{u_r^*}{\sigma_\Theta}. \quad (7)$$

The benefit of this normalisation becomes clear below and it should be noted that this normalisation can be applied without loss of generality in scaling features. This fact can be easily shown, for instance with eq. (3) and (4), where a multiplication with an arbitrary factor does not change the scaling exponent.

3.2 Multi-scale analysis

The characterisation with structure functions can be expressed by unconditional probability density functions $p(u_r)$,

$$S^\kappa(r) = \int_{-\infty}^{+\infty} u_r^\kappa p(u_r) du_r. \quad (8)$$

Thus, all structure functions are equivalent to the information of $p(u_r)$, cf. Frisch (2001). However, a more general description of the cascade stochastics is a N -scale joint PDF $p(u_r; u_{r+\Delta}; u_{r+2\Delta}; \dots; u_{r+N\Delta})$, which captures the entire multi-scale characteristic, cf. Friedrich and Peinke (1997).

Earlier studies show that the turbulent cascade process and its increment series, respectively, has the Markov property, e.g. Friedrich and Peinke (1997); Renner et al. (2001, 2002); Tutkun and Mydlarski (2004); Lück et al. (2006). Thus, general joint PDF can be expressed by conditional PDFs,

$$p(u_r; u_{r+\Delta}; \dots; u_{r+N\Delta}) = p(u_r | u_{r+\Delta}) p(u_{r+\Delta} | u_{r+2\Delta}) \times \dots \times p(u_{r+(N-1)\Delta} | u_{r+N\Delta}) p(u_{r+N\Delta}). \quad (9)$$

Motivated by the cascade picture, an increment u_r is conditioned on an increment on a larger scale $u_{r+\Delta}$. The Markov property is valid in case of $\Delta \geq l_{EM}$, where l_{EM} is the Einstein-Markov coherence length and according to $l_{EM} \propto \lambda$, cf. Lück et al. (2006); Stresing et al. (2012). Unless stated otherwise we take the step width in the cascade as $\Delta = l_{EM} = 2\lambda$. Details of the determination of the Einstein-Markov coherence length are given in the appendix A2.

Thus, the stochastic process at scale r is determined by the conditional PDF $p(u_r | u_{r+l_{EM}})$ and the entire cascade can be described by $p(u_r | u_{r+l_{EM}})$ as function of r . Note, the Einstein-Markov coherence length introduces a coarse-graining or discretisation of the turbulent cascade so that the stochastic approach becomes feasible. (As a remark we mention that already Einstein (1905) discussed the need of such a concept in his pioneering work on Brownian motion.)

Starting from an initial distribution, e.g. at the integral length scale $p(u_L)$ or any other starting scale r' , the evolution of $p(u_r | u_L)$ can be described by the Fokker-Planck equation (also known as Kolmogorov equation), cf. Friedrich and Peinke (1997); Renner et al. (2001),

$$-\frac{\partial}{\partial r} p(u_r | u_{r'}) = -\frac{\partial}{\partial u_r} \left[D^{(1)}(u_r) p(u_r | u_{r'}) \right] + \frac{\partial^2}{\partial u_r^2} \left[D^{(2)}(u_r) p(u_r | u_{r'}) \right]. \quad (10)$$

Thereby any $p(u_r | u_{r'})$ with $r < r'$ can be obtained. The functions $D^{(1)}(u_r)$ and $D^{(2)}(u_r)$ govern the Fokker-Planck equation and are named drift and diffusion function and more generally first and second Kramer-Moyal coefficient. The Fokker-Planck equation is a truncated Kramers-Moyal expansion Risken (1984), where only the first two terms are considered. Due to the fact that the first two terms of the Kramers-Moyal expansion strongly dominate the expansion, cf. Renner et al. (2001); Tutkun and Mydlarski (2004), the description of conditional PDFs evolution in scale is justified by the Fokker-Planck equation. This dominance can be related to Pawula's theorem, which justifies the Fokker-Planck equation, cf. Risken (1984).

The Fokker-Planck approach can be related to the characterisation of structure functions by partial integration of eq. (10), e.g. Renner et al. (2001),

$$-r \frac{\partial}{\partial r} S^\kappa(r) = r \kappa \langle u_r^{\kappa-1} D^{(1)}(u_r) \rangle + r \kappa (\kappa - 1) \langle u_r^{\kappa-2} D^{(2)}(u_r) \rangle. \quad (11)$$

It is easily seen that this set of equation for S^κ gets unclosed if drift and diffusion terms have higher order contributions in u_r ($D^{(1)}$ higher than linear, $D^{(2)}$ higher than quadratic).

3.3 Estimation of Kramers-Moyal coefficients

Kramers-Moyal coefficients can be estimated by conditional moments,

$$M^{(\kappa)}(\tilde{u}_r, \delta) = \int_{-\infty}^{+\infty} (\tilde{u}_r - \tilde{u}_r')^\kappa p(u_r | u_r') d\tilde{u}_r, \quad (12)$$

$$= \langle [u_r - u_r']^\kappa \rangle_{|u_r'} \quad (13)$$

$$D^{(\kappa)}(u_r) = \lim_{\delta \rightarrow 0} \frac{1}{\kappa! \delta} M^{(\kappa)}(u_r, \delta), \quad (14)$$

where κ is the order of the coefficient, cf. Risken (1984) and $\delta = r' - r$. A common method to estimate $\lim_{\delta \rightarrow 0}$ in eq. (14) is an extrapolation. The evolution of moments $M^{(\kappa)}(u_r, \delta)$ between $\delta = l_{EM}$ and $\delta = 2l_{EM}$ is linearly extrapolated to $\delta = 0$ and the crossing with the ordinate axis estimates the limit, for further details on this limit see Renner et al. (2001); Gottschall and Peinke (2008); Honisch and Friedrich (2011). The limit approximation leads to uncertainties, whereas the functional form of Kramers-Moyal coefficients are commonly well estimated. An optimisation procedure is used to minimise possible uncertainties, which was proposed in Nawroth et al. (2007); Kleinhans et al. (2005).

Four steps are necessary for this optimisation: i) parameterisation of Kramers-Moyal coefficients, ii) calculation of $p(u_r; u_{r+l_{EM}})$, iii) estimating the difference between calculated distribution $p(u_r; u_{r+l_{EM}})$ and measured joint PDF and iv) an iterative optimisation procedure finds best fitting Kramers-Moyal coefficients, which lead to a minimal distance between the distributions.

Next the four steps are discussed in details: *Step i)* A common parameterisation (d_{ij}) of the Kramers-Moyal coefficients is a linear function for $D^{(1)}$ and a parabola function for $D^{(2)}$

$$D^{(1)}(u_r) = d_{11}(r) u_r, \quad (15)$$

$$D^{(2)}(u_r) = d_{22}(r) u_r^2 + d_{20}(r). \quad (16)$$

These functions conform well to the shape of $D^{(1)}$ and $D^{(2)}$ ($D^{(1,2)}$), see also below.

Step ii) A calculation of $p(u_r | u_{r+l_{EM}})$ is done by the use of the short time propagator (Riskin, 1984, p. 73, eq. (4.55))

$$p_{STP}(u_r | u_{r+l_{EM}}) \approx \frac{1}{\sqrt{4\pi D^{(2)}(u_{r+l_{EM}})}} \times \exp\left(-\frac{[u_r - u_{r+l_{EM}} - D^{(1)}(u_{r+l_{EM}})]^2}{4D^{(2)}(u_{r+l_{EM}})}\right). \quad (17)$$

This particular functional form of eq. (17) is reached by implementing the scale step l_{EM} in unites of Einstein-Markov coherence length, which has the advantage that the short time propagator depends only on $D^{(1,2)}$.

It was investigated by the use of the Chapman-Kolmogorov equation, cf. Risken (1984), how small a scale step might be. The specified step size leads to a proper results, smaller steps than l_{EM} do not significantly improve results.

Since the experimentally found conditional PDFs $p_{exp}(u_r | u_{r+l_{EM}})$ become noisy for large values of u_r and $u_{r+l_{EM}}$ it is better to use the joint PDFs for the optimisation procedure. Therefore conditional PDFs $p_{STP}(u_r | u_{r+l_{EM}})$ from eq. (17) get converted by Bayes' theorem to joint PDFs $p_{STP}(u_r; u_{r+l_{EM}})$.

Step iii) Next we set the numerical calculated joint PDF p_{STP} in comparison with the measured reference p_{exp} by the use of a weighted mean square error function in logarithmic space, cf. Feller (1968), (analogous to Kullback-Leibler entropy),

$$\varepsilon(p_{STP}, p_{exp}) = \frac{\int_{-\infty}^{+\infty} \int_{-\infty}^{+\infty} (p_{STP} + p_{exp})(\ln(p_{STP}) - \ln(p_{exp}))^2 du_r^2}{\int_{-\infty}^{+\infty} \int_{-\infty}^{+\infty} (p_{STP} + p_{exp})(\ln^2(p_{STP}) + \ln^2(p_{exp})) du_r^2}, \quad (18)$$

with \ln as natural logarithm. ε is taken as a logarithmic measure for the distance between the distributions.

Step iv) By means of an optimisation process, $D^{(1,2)}$ get systematically changed until the cost function ε is minimised. The optimisation procedure is a 2nd order method based on a Hessian matrix. We used for this optimisation the in MATLAB[®] R2012a implemented function *fmincon*. The constraints are set in a physically and mathematically meaningful way, $-\infty \leq d_{11} \leq 0$, $0 \leq d_{22} \leq \infty$ and $0 < \delta_d \leq d_{20} \leq \infty$, here $\delta_d = 10^{-3}$.

The procedure, explained here, optimises the Kramers-Moyal coefficients for different r values on the basis of $p(u_r | u_{r+l_{EM}})$ along the inertial range. Using the same procedure but for one fixed condition, e.g. at a large scale L or $p(u_r | u_L)$, leads to the same results of $D^{(1,2)}$.

3.4 Integral fluctuation theorem

Next we present an independent measure to quantify the quality of estimated functions $D^{(1,2)}$. Here, Kramer-Moyal functions describe the turbulent system and increment trajectories from an initial state given by $p(u_L)$ to a final state $p(u_\lambda)$.

The evolution in scale of increments is interpreted as a non-equilibrium thermodynamics, for which new fundamental laws were found by Jarzynski (1997). In particular, concerning entropy production of the cascade process. From these laws Seifert (2005) derived the integral fluctuation theorem (IFT). Nickelsen and Engel (2013) showed for free jet flow data that the IFT is fulfilled for the turbulent cascade and they conclude: “*The integrated fluctuation theorem for entropy production represents an extremely sensitive indicator for the precise modeling of small-scale intermittency.*”

Two interesting points rise for our work, on the one side we can show that this fundamental thermodynamical law holds for different generated turbulent flows, and thus it might be a universal feature of turbulence. On the other side the high sensitivity of IFT can be used to quantify the importance and significance of different functional contributions to $D^{(1,2)}$.

To test the quality of the estimated functions $D^{(1,2)}$ the entropy production of velocity increments is considered along their scale path through the turbulent cascade. To denote a single path or trajectory of velocity increments, we define $u(\cdot) = \{u_r; r = L, \lambda\}$, which is selected at a fixed x . Another path can be determined by changing the position x . In order to get independent paths the change in x is taken to be equal to L . The entropy production for a single path $u(\cdot)$ can be calculated from the functional, cf. Nickelsen and Engel (2013),

$$\Delta S[u(\cdot)] = - \int_L^\lambda \partial_r u_r \partial_u \varphi(u_r) dr - \ln \frac{p(u_\lambda, \lambda)}{p(u_L, L)} \quad (19)$$

with the non-equilibrium potential

$$\varphi(u_r) = \ln D^{(2)}(u_r) - \int_{-\infty}^{u_r} \frac{D^{(1)}(\tilde{u}_r)}{D^{(2)}(\tilde{u}_r)} d\tilde{u}_r. \quad (20)$$

Here u_L and u_λ denote velocity increments at the *initial* and *final* state. The produced entropy ΔS along these paths can be positive or negative. The integral fluctuation theorem, cf. Seifert (2005),

$$\langle e^{-\Delta S} \rangle_n = 1 \quad (21)$$

determines a general balance of the entropy production, in the case many trajectories are considered. For the fulfilment of the IFT, velocity increments u_r , the probabilities $p(u_L)$ and $p(u_\lambda)$, as well as the coefficients $D^{(1,2)}$ have to be in exact balance. Thus, quantities taken directly from the measured data and the stochastic process describing coefficients $D^{(1,2)}$ are compared with the IFT. Only if $D^{(1,2)}$ properly characterise the turbulent cascade the IFT is fulfilled. Vice versa, if the general validity of the IFT is assumed, a criterium is given for $D^{(1,2)}$. With other words we claim that if the IFT is fulfilled, $D^{(1,2)}$ describe the stochastic cascade process correctly. This sensitivity is used in the following to verify the accuracy of $D^{(1,2)}$. Furthermore, the IFT is used to prove how many parameters are necessary for $D^{(1,2)}$, see eq. (15) and (16). Note, a continuous $D^{(1,2)}$ is necessary in order to determine the IFT, therefore $D^{(1,2)}$ are fitted by polynomial up to 5th order. These coefficients are fitted in scale between l_{EM} and L .

4 Results

In this section we show results, which we obtained from our datasets. The analysis of structure functions sets our data into the common picture of turbulence and checks if the data obey a scaling law. Subsequently, results to the IFT are shown, to prove the general validity of the IFT and of our parameterisation of Kramers-Moyal coefficients. Thereafter, results of multi-scale statistics are presented and discussed in the context of the question of universal and non-universal flow dependencies of turbulence.

4.1 2-point scaling features

Figure 1 presents second ($\kappa = 2$) and fourth ($\kappa = 4$) order structure functions according to eq. (3) obtained from all 61 datasets. The lower band corresponds to second and the upper band corresponds to fourth structure functions. The greyscale of the curves indicates the Taylor Reynolds numbers. It is clearly seen how the *scaling range* increases with the Reynolds number. Structure functions are normalised in their scale and in their values by Θ and σ_Θ , defined in section 3.1. The band of the fourth structure functions is shifted by a factor of 10 along the ordinate axis for reason of presentation. The norms Θ and σ_Θ are shown in the appendix A3 as function of Re_λ . These norms are dimensional and show features, which depend on the *flow type*.

For a more precise analysis of the scaling behavior of the structure functions we present in Figure 2 a) the local scaling exponent $\xi_2(r)$, eq. (6). Due to our normalisation all datasets pass through $\xi_2 = 0.696$ at $\frac{r}{\Theta} = 1$. Three curves for exemplary Reynolds numbers are marked by symbols to indicate that $\xi_2(r)$ changes from a linear behavior for low Re -numbers to a *power 5* behavior for high Re -numbers (with respect to the log-log presentation). This shows that the local scaling exponent flattens with increasing Re_λ around $\xi_2 = 0.696$. Thus, only a tendency to proper scaling behavior is seen, but there is no stretched constant scaling range, even for the highest Re_λ datasets. (With proper scaling we refer to the case that no functional deviation from a scaling law is present, i.e. $\xi_\kappa(r)$ is rigorously constant in r , e.g. eq. (5).) For the third and fourth structure function Sinhuber (2015, pp. 121-122, fig. 4.3 and 4.4) shows similar results and confirm the flattening of structure functions for even higher Re_λ for grid generated turbulence, also Grauer et al. (2012) used a

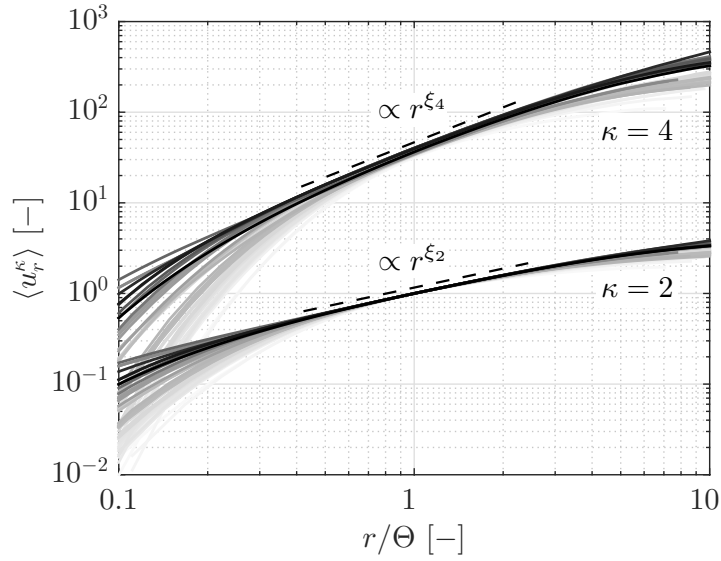


Figure 1: Second ($\kappa = 2$, lower band) and fourth ($\kappa = 4$, higher band) order structure functions over normalised scale. The whole band of the fourth structure functions is shifted by a factor of 10 for reason of presentation. The greyscale used for the curves indicates corresponding Taylor Reynolds numbers, bright grey to black corresponds to increase of Re_λ

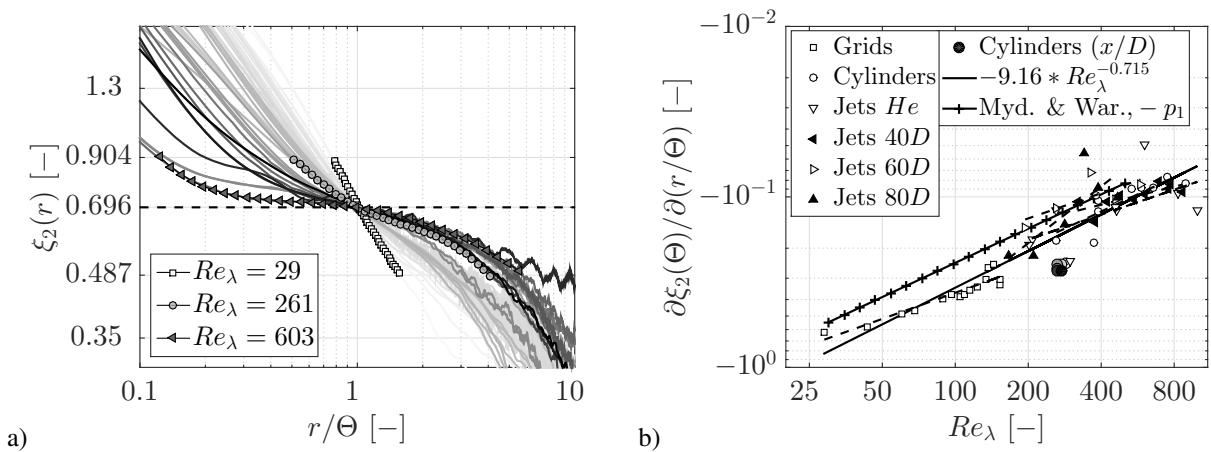


Figure 2: a) Local second order scaling exponent $\xi_2(r)$ according to eq. (6) in a double logarithmic plot. Presentation alike figure 1. b) Slope of local second order scaling exponent $\xi_2(r)$ at $r = \Theta$ in a double logarithmic presentation together with data from Mydlarski and Warhaft (1996)

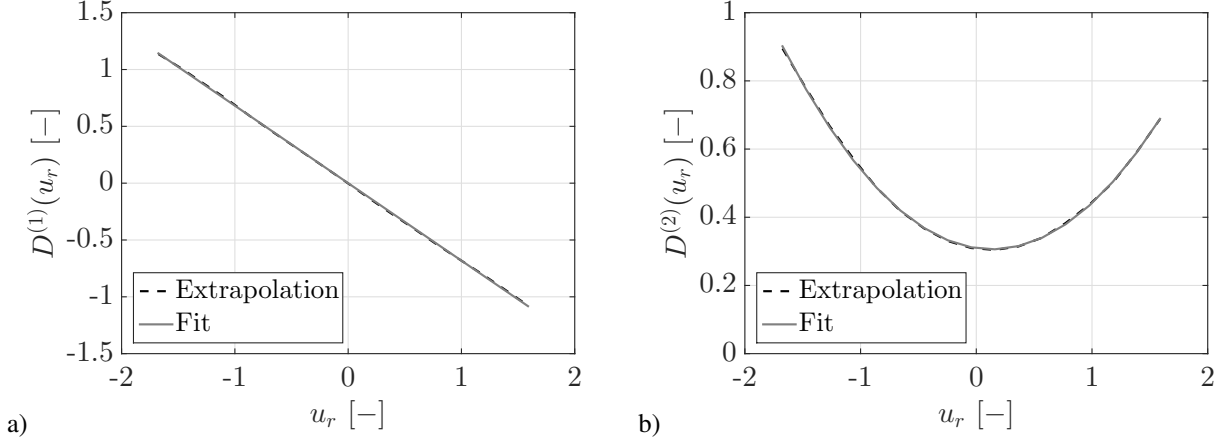


Figure 3: $D^{(1,2)}$ over u_r , according to eq. (14) and cf. Gottschall and Peinke (2008). Linear and parabola fitting functions illustrate their functional form. The dataset *jet 1* (table 1) is used at $r = 1l_{EM}$

similar approach.

Figure 2 b) shows the slope of local second order scaling exponent $\xi_2(r)$ at $r = \Theta$ as function of Re_λ . This slope is obtained from a fitting with an polynomial of the 5th order as shown in fig. 2 a). The solid line shows the trend of all datasets with the functional form of

$$\frac{\partial \xi_2(\Theta)}{\partial (r/\Theta)} \approx -9.16 Re_\lambda^{-0.715}. \quad (22)$$

Based on this result, $\partial_{(r/\Theta)} \xi_2(\Theta)$ can be proposed as an alternative to Re_λ .

Additional data from Mydlarski and Warhaft (1996) are added to figure 2 b), as they did a similar study, where a correction p_1 to the proper scaling of energy density spectra $E(k)$ was investigated as function of Re_λ , up to 500. (Note, second order structure function and energy density spectra contain the same information and can be converted into each other by Fourier transformation.) For $E(k) \propto k^{-(5/3-p_1)}$ they found that p_1 has the form $p_1 = 5.25 Re_\lambda^{-2/3}$, which is very similar to our found Re_λ -dependence, eq. (22). The pre-factor differ due to different normalisations.

Besides the scattering of our data, no remarkably different behavior of the different subgroup data can be found, thus we conclude that this 2-point analysis, fig. 1, 2 a) and b), supports the common view of universal scaling features of structure functions.

4.2 Estimation procedure of Kramers-Moyal coefficients

The first estimation of Kramer-Moyal coefficients is based on conditional moments and their extrapolation. Figure 3 a) and b) show exemplary $D^{(1)}$ and $D^{(2)}$ as function of u_r , according to eq. (14). A linear and a parabola fitting function show the common functional forms of $D^{(1,2)}$, which is used for the subsequent optimisation. The used fit range is indicated, $-1.5 \leq u_r \leq 1.5$. Here one might argue that higher order contributions can be seen in $D^{(1,2)}$. To this point we come back below, when results of the IFT are shown. These Kramers-Moyal coefficients deduced by moments lead to a rather imprecise description of the turbulent cascade and the reconstruction of conditional PDFs via eq. (17) is improvable, even if higher order corrections are used, see Risken (1984, p. 66, eq. (4.12)) and discussions of this problem in Gottschall and Peinke (2008, eq. (6a) and (6b)) and Renner (2002, p. 37, eq. (4.13) and p. 65, eq. (6.13)).

As a second step for the estimation of Kramer-Moyal coefficients, the optimisation procedure of Chapter 3.3 is applied. This procedure is based on the reconstruction of PDFs according to eq. (17). Figure 4 shows the quality of reconstructing conditional PDFs by the optimised Kramers-Moyal coefficients at two different scales, $r = l_{EM}$ and $r = 60l_{EM}$. To pronounce differences we have chosen $r = 60l_{EM}$, which corresponds to a scale large than L . The agreement of experimental and reconstructed conditional PDFs is good.

Due to the fact that the reconstructed conditional PDF is strictly symmetric, an *asymmetric* experimental conditional PDF leads to a mismatch, which can be seen for the outer parts of the distribution, fig. 4. Due to the functional form of the short time propagator, eq. (17), the mentioned deviations can not be taken into account, with other words a better matching can not be realised between experimental and reconstructed conditional PDF.

In order to further show the quality of the reconstructing conditional PDF, we analyse the change of conditional PDF

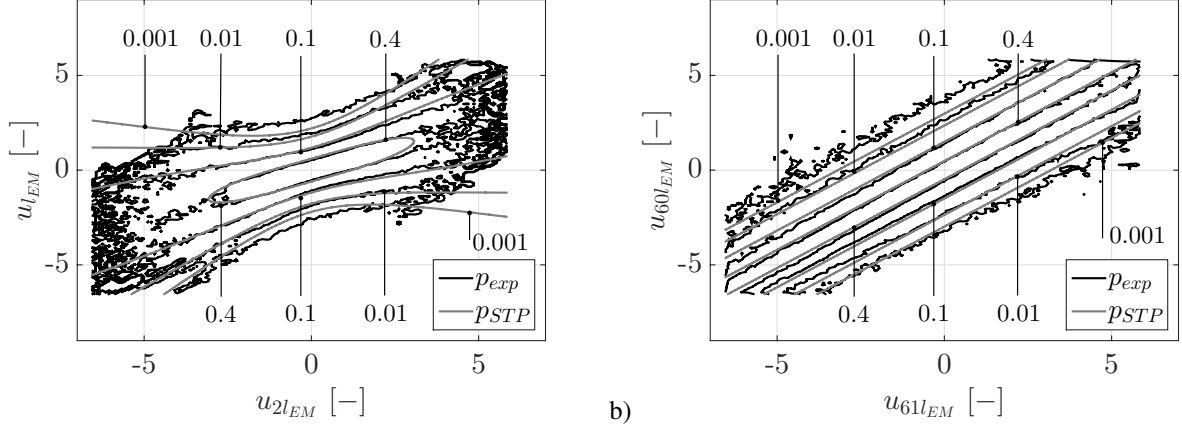


Figure 4: Contour plots show experimental and reconstructed conditional PDFs at two different scales, a) $r = l_{EM}$ and b) $r = 60l_{EM}$. A dataset of subgroup (v) is used with $Re_\lambda = 475$

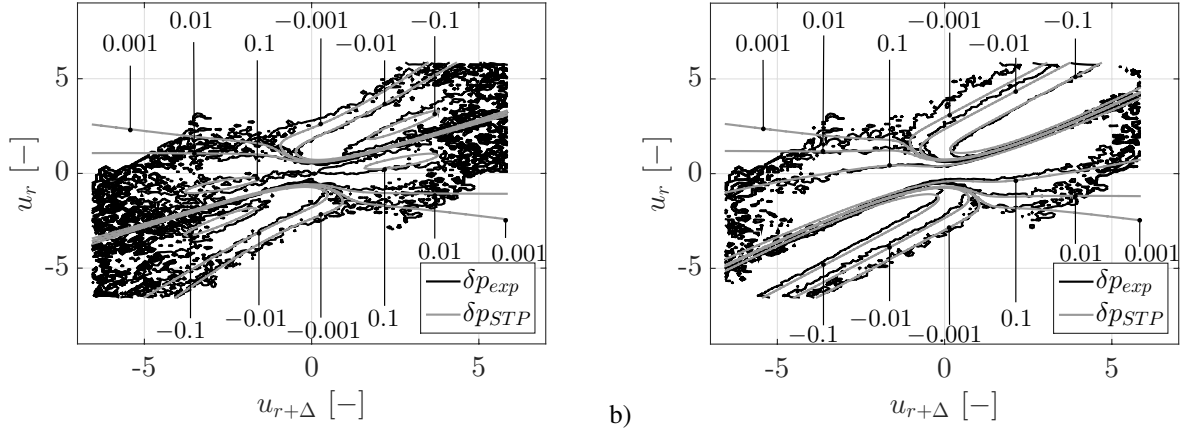


Figure 5: Change of conditional PDF δp along the scale. a) δp for $N = 2$, which corresponds to small scale change and b) for $N = 60$, which corresponds to the entire change within inertial range. A dataset of subgroup (v) is used with $Re_\lambda = 475$

along the scale, cf. eq. (9). Figure 5 shows the cumulative change of conditional PDF, expressed as

$$\begin{aligned} \delta p &= [p(u_{l_{EM}}|u_{2l_{EM}}) - p(u_{2l_{EM}}|u_{3l_{EM}})] \\ &+ [p(u_{2l_{EM}}|u_{3l_{EM}}) - p(u_{3l_{EM}}|u_{4l_{EM}})] \\ &+ \dots \\ &+ [p(u_{(N-1)l_{EM}}|u_{Nl_{EM}}) - p(u_{Nl_{EM}}|u_{(N+1)l_{EM}})] \end{aligned} \quad (23)$$

$$= p(u_{l_{EM}}|u_{2l_{EM}}) - p(u_{Nl_{EM}}|u_{(N+1)l_{EM}}). \quad (24)$$

δp_{exp} corresponds to the cumulative change of experimental data and δp_{STP} is deduced by means of the short time propagator and the optimised Kramers-Moyal coefficients. Due to the scale wise optimisation procedure, eqs. (23) and (24) are not necessarily equal for the reconstructed PDFs, thus we use eq. (23). Figure 5 a) shows δp for $N = 2$, the change of the conditional PDF at small scales and figure 5 b) presents δp for $N = 60$. We see in both figures that the distributions of δp_{exp} and δp_{STP} are in good agreement. Thus, the optimisation procedure works well from the smallest scale changes $\delta r = l_{EM}$ up to the cumulative change of the entire inertial range. Consequently we assume that the description of the turbulent cascade process is properly characterised by optimised Kramers-Moyal coefficients.

4.3 Parameterisation of $D^{(1,2)}$ and general validity of the integral fluctuation theorem

As a next step we test the validity of the IFT as a feature of non-equilibrium thermodynamics. Figure 6 presents the IFT for all 61 datasets as a function of the number of considered velocity increment trajectories n , i.e. independent cascade paths. Here we used the optimised coefficients $D^{(1,2)}$, parametrised according to eqs. (15) and (16). Due to different

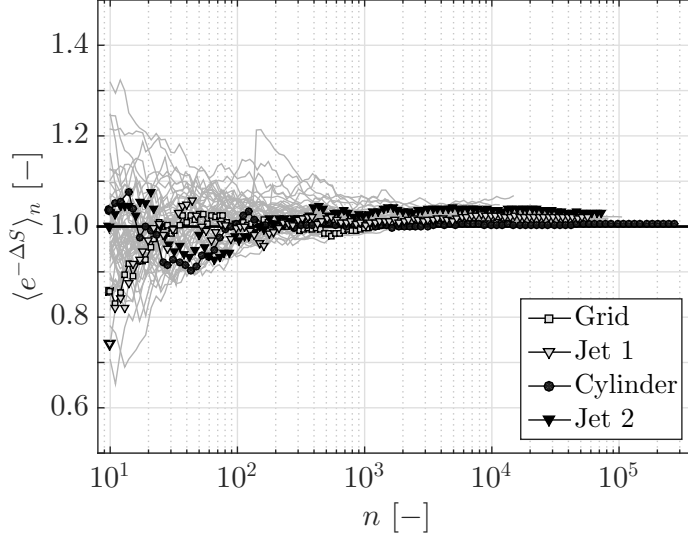


Figure 6: IFT according to eq. (21) as a function of the number of trajectories n . Results from all data; highlighted by bold symbols the selected datasets from table 1, all the others are shown as grey lines

P	d_{13}	d_{12}	d_{11}	d_{10}	d_{23}	d_{22}	d_{21}	d_{20}	I_{max}
2a	-	-	X	-	-	-	-	X	$1.3(46) \pm 0.016$
2b	-	-	X	-	-	X	-	-	∞
3	-	-	X	-	-	X	-	X	$1.0(17) \pm 0.016$
4	-	-	X	X	-	X	-	X	$1.0(17) \pm 0.016$
5	-	-	X	X	-	X	X	X	$1.0(18) \pm 0.016$
6	-	X	X	X	-	X	X	X	$1.0(21) \pm 0.016$
7	X	X	X	X	-	X	X	X	$1.0(21) \pm 0.016$
8	X	X	X	X	X	X	X	X	$1.0(24) \pm 0.016$

Table 2: Scheme of the chosen parameters d_{ij} for $D^{(1,2)}$ according to eqs. (25) and (26). On the left row the number of used parameters are given. Crosses indicated non-zero parameters. The corresponding I_{max} values are given with their uncertainties

numbers of samples in the datasets and varying Taylor micro-scale as well as integral lengths, the maximal number of independent trajectories differ from dataset to dataset. The four selected datasets from table 1 are highlighted by bold symbols, other datasets are shown in grey. It is clearly seen that after averaging over $n \approx 1000$ trajectories the averaged entropy values converge to 1 as predicted by the IFT, eq. (21). The average of the 61 IFT values taken at maximal n is $\langle \langle e^{-\Delta S} \rangle_{n=max} \rangle_{datasets} = \langle I_{max} \rangle \approx 1.01$ and their standard deviation is $\sigma(I_{max}) \approx 0.01$, which we take as a strong hint that the IFT is a fundamental thermodynamical law for the turbulent cascade. Note, it is the first time that such a large turbulent flow dataset conforms with the IFT, what shows the general meaning of the findings by Nickelsen and Engel (2013).

Taking this IFT as a fundamental law, we can verify which parameterisation of the coefficients $D^{(1,2)}$ are allowed. Furthermore, essential functional contributions to $D^{(1,2)}$ can be investigated and found. To test these aspects we parameterise the coefficients up to third order in u_r , i.e. with 8 parameters,

$$D^{(1)}(u_r) = d_{13}(r)u_r^3 + d_{12}(r)u_r^2 + d_{11}(r)u_r + d_{10}(r), \quad (25)$$

$$D^{(2)}(u_r) = d_{23}(r)u_r^3 + d_{22}(r)u_r^2 + d_{21}(r)u_r + d_{20}(r). \quad (26)$$

These 8 parameters were varied in a systematic way as shown in table 2 and in figure 7 for one exemplary dataset (subgroup (v), $Re_\lambda = 475$). For each selection of parameters the above mentioned optimisation procedure was repeated. The IFT theorem was tested for the obtained optimised parameters of $D^{(1,2)}$. The resulting values I_{max} are shown in table 2. We estimate an error of the I_{max} by considering the convergence of the IFT and its fluctuations around the saturating value I_{max} , fig. 7. In accordance with the mentioned standard deviation ($\sigma(I_{max}) \approx 0.01$), the estimated error (namely the magnitude of the final IFT fluctuations) is 0.016. From the results presented in table 2 and in fig. 7 we conclude that different functional representations of $D^{(1,2)}$ are possible to fulfill the IFT in good quality.

Next we discuss the meaning of the single cases. The case $P = 2a$, of table 2, corresponds to pure additive noise in the cascade process, so that only Gaussian increment distributions would be expected. The value of $I_{max} = 1,3(46)$ and the big jumps with n (see fig. 7) clearly show that the IFT can not be well fulfilled with this functional ansatz, which we

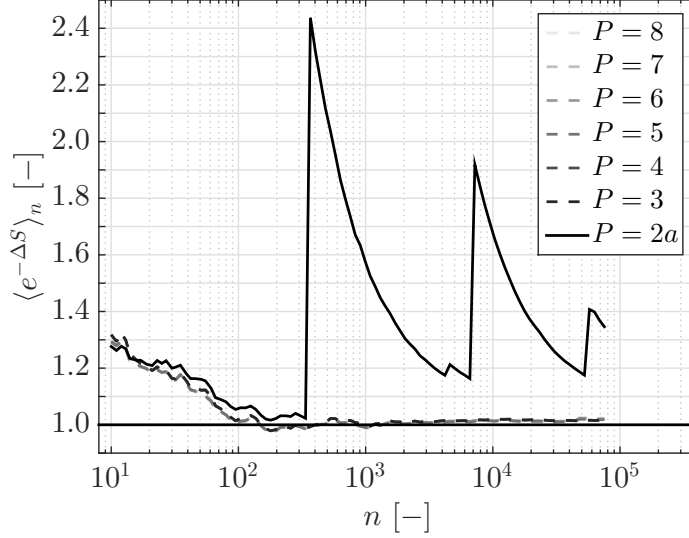


Figure 7: IFT, according to eq. (21), as function of the number of trajectories n for different parameterisation of $D^{(1,2)}$ according to table 2. Note, case $P = 2b$ is not shown in fig. 7, since the IFT diverges for this case

consequently rejected as a functional form of $D^{(1,2)}$.

The case $P = 2b$ corresponds to pure multiplicative noise in the cascade process. Note, this parameterisation corresponds to the scaling proposed by Kolmogorov, see eq. (5) and Friedrich and Peinke (1997). Also this functional form of $D^{(1,2)}$ is rejected as the IFT diverges.

For all the other choices with three and more parameters ($P \geq 3$), we see good fulfillment of the IFT. More coefficients do not lead to a significantly better fulfillment of the IFT and in its convergence. From this we conclude that the case $P = 3$ is sufficient for a good stochastic model for the turbulent cascade. Higher order terms as used in Renner et al. (2001) and Nickelsen and Engel (2013) seem not to be necessary.

Note, $D^{(1)}$ and $D^{(2)}$ estimated from conditional moments, fig. 3, gives already an good indication of the functional form, which is confirmed on the basis of the IFT. However, $D^{(2)}$ deduced by moment indicates a d_{21} unequal to zero, (d_{21} shifts the $D^{(2)}$ -parabole off zero). In contrast, the very sensitive IFT in combination with the optimisation procedures show that this shift is negligible in the stochastic description of the turbulent cascade. We also recognised that d_{22} becomes increasingly important for the fulfillment of the IFT with increasing Re_λ .

The need of the three parameters can be discussed in the context of structure functions see Section 3.2 and eq. (11). Inserting the three parameters and a multiplication by $-\frac{r}{S^\kappa}$ (from the left) lead to

$$\xi_\kappa = \frac{r}{S^\kappa} \frac{\partial S^\kappa}{\partial r} = -r\kappa \left(d_{11}(r) + (\kappa - 1) \left(d_{22}(r) + \frac{S^{(\kappa-2)}(r)}{S^\kappa(r)} d_{20}(r) \right) \right). \quad (27)$$

Here, we used the substitution $\frac{r}{S} \frac{\partial S}{\partial r} = \frac{\partial \ln(S)}{\partial \ln(r)} = \xi_\kappa(r)$, see eq. (6).

It is obvious that if more parameters were needed, eq. (27) becomes more complicate. In the case of negligible d_{20} , eq. (27) is an analytic expression for $\xi_\kappa(r)$ and can be transformed in a form comparable to Kolmogorov's expression of the scaling exponent, eq. (5), if d_{11} and d_{22} are constants, cf. Renner et al. (2001). The need for the three parameters still has the consequence that this coupled set of differential equations (27) is closed. Knowing starting conditions (e.g. Θ and σ_Θ) as well as $S^0 = 1$ and $S^1 = 0$ all higher structure functions can be determined successively. The consistency of the determined coefficients with the measured structure functions is shown in appendix A4. Furthermore, $d_{20} \neq 0$ and $d_{22} \neq 0$ can be interpreted for the turbulent cascade as a necessary combination of additive and multiplicative noise, which can be also related to the energy cascade as discussed in Ch. Renner (2013).

4.4 The turbulent cascade in terms of Kramers-Moyal coefficients

Based on the presented results we assume from now on the validity of the IFT as a general law for turbulence. Furthermore, we will estimate the Kramers-Moyal coefficients with the simplest functional form as worked out in section 4.3. The aim of the discussion will be to see how far the parameters $d_{11}(r)$, $d_{20}(r)$ and $d_{22}(r)$ behave in a universal way with respect to dependencies on the Reynolds number and on the flow type.

Before the results of Kramers-Moyal coefficients are discussed in details, figure 8 illustrates which influence the form of the conditional PDFs have on the parameters $d_{11}(r)$, $d_{20}(r)$ and $d_{22}(r)$. Figure 8 a) shows an exemplary conditional PDF at a small scale, $r = l_{EM}$. The maximum of the distribution is located at the diagonal, which follows the function

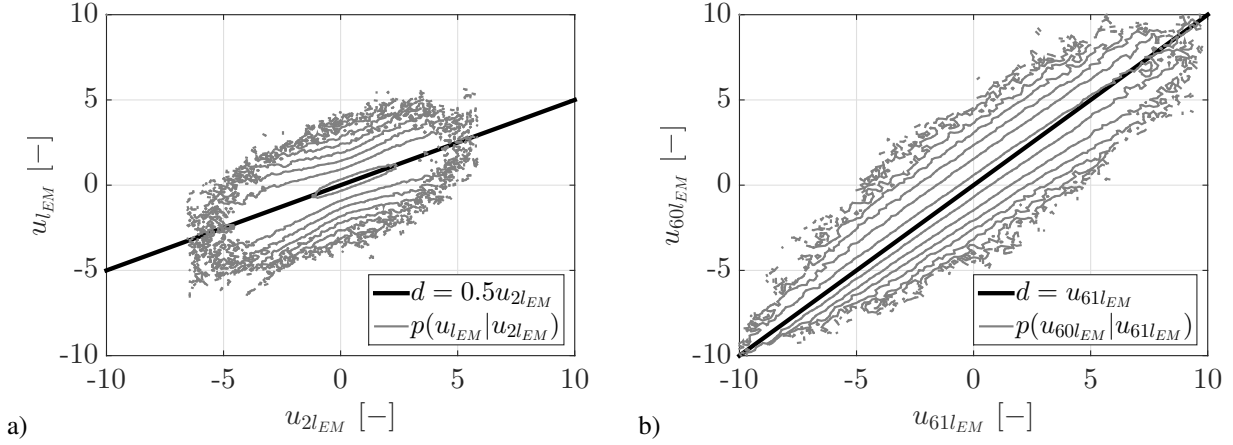


Figure 8: a) Conditional PDF at $r = l_{EM}$, the diagonal of the PDF and its location is indicated by the function $d = 0.5u_{2l_{EM}}$. b) Conditional PDF at $r = 60l_{EM}$, the diagonal function is $d = u_{61l_{EM}}$. For a) and b) a dataset of subgroup (v) is used with $Re_\lambda = 475$

$d = 0.5u_{2l_{EM}}$ and will be named in the following *distributions diagonal* or simply *diagonal*. The contour isolines are curved beneath and above this diagonal.

Figure 8 b) shows for the same dataset the conditional PDF at larger scale, $r = 60l_{EM}$. To pronounce differences from small and large scale $r = 60l_{EM}$ is chosen larger than L . The distributions diagonal is now roughly at $d = u_{61l_{EM}}$. The contour isolines are not any more curved but almost parallel to the diagonal.

These changes in conditional PDF shape can be understood by considering the short time propagator, eq. (17). The leading term for the maximum is given by $D^{(1)}$ and d_{11} . The smaller the magnitude of d_{11} the more the diagonal becomes $d = u_{r+l_{EM}}$. The width w of the distribution around the diagonal is proportional to the denominator in the exponential term of eq. (17), $w \propto d_{20} + d_{22} u_{r+l_{EM}}^2$. Thus, coefficient d_{22} expresses the nonlinearity in the standard deviation and gives rise to the curvature of the contour isolines. The lower d_{22} the smaller the curvature will be. In terms of unconditional PDF, a big d_{22} is equivalent to fat-tailed PDF distributions. At $u_{r+l_{EM}} = 0$, d_{20} characterises the width of the distribution. Further details are discussed in appendix A5.

Next we return to the discussion of the scale dependence of the three parameters d_{11} , d_{22} and d_{20} . In figure 9 these parameters are shown as a function of the scale r and the Taylor based Reynolds number Re_λ for grid generated turbulence. Grid data were selected as for these the smallest scattering was observed. (Results of the parameters for cylinder and free jet flows are shown in appendix A6.)

Figure 9 a) shows the convergence of all d_{11} to the fixed value $d_{11} = -0.5$ at $r = l_{EM}$, which corresponds to a distribution diagonal $d = 0.5u_{r+l_{EM}}$, like figure 8 a). Furthermore, all d_{11} are approximately linear at small scales. Thus, d_{11} can be expressed according to,

$$d_{11} \approx -0.5 \left(\frac{r}{l_{EM}} \right)^{-\frac{1}{2}}. \quad (28)$$

Eq. (28) is quite universal, since it is also found for the other flows, as shown below. This findings is in accordance with Renner et al. (2002), where d_{11} of free jet flows was also parameterised and an equivalent scaling behavior with the exponent $(-\frac{1}{2})$ was found. At larger scales, $r \leq 4l_{EM}$, deviations from the power law become visible, d_{11} bends down relative to the power law. The higher Re_λ the larger the scale at which the bending regime appears. Thus, eq. (28) indicates that the case $d = u_{r+l_{EM}}$ is reached only at very large scales and in the limit of very large Re_λ .

Figure 9 b) presents d_{20} in a semi-logarithmic plot. All d_{20} show a similar functional form with an increase with scale and with a small monotone curvature. The Re_λ -dependency is rather weak. The functional form can be approximated by

$$d_{20} \approx \left(\alpha_{20} \ln \left(\frac{r}{l_{EM}} \right) + \beta_{20} \right)^{\frac{1}{3}}, \quad (29)$$

where α_{20} and β_{20} are fit parameters, see also A4 and figure 15 c).

Figure 9 c) presents d_{22} in a semi-logarithmic plot. All d_{22} decrease strongly with increasing scale. This decrease slows down with increasing Re_λ . This functional behavior can be approximated by

$$d_{22} \approx \alpha_{22} \ln \left(\frac{r}{l_{EM}} \right) + \beta_{22}, \quad (30)$$

where α_{22} and β_{22} are fit parameters, see also A4 and figure 15 b).

Figure 10 shows an overview for the three parameters and for all data. The parameters are sorted in three groups, which respect the different turbulent flow types. All parameters which belong to grid flows, to cylinder flows or to free jet flows are covered by a surfaces with different greyscale and are surrounded by different symbols. Dashed lines indicate where

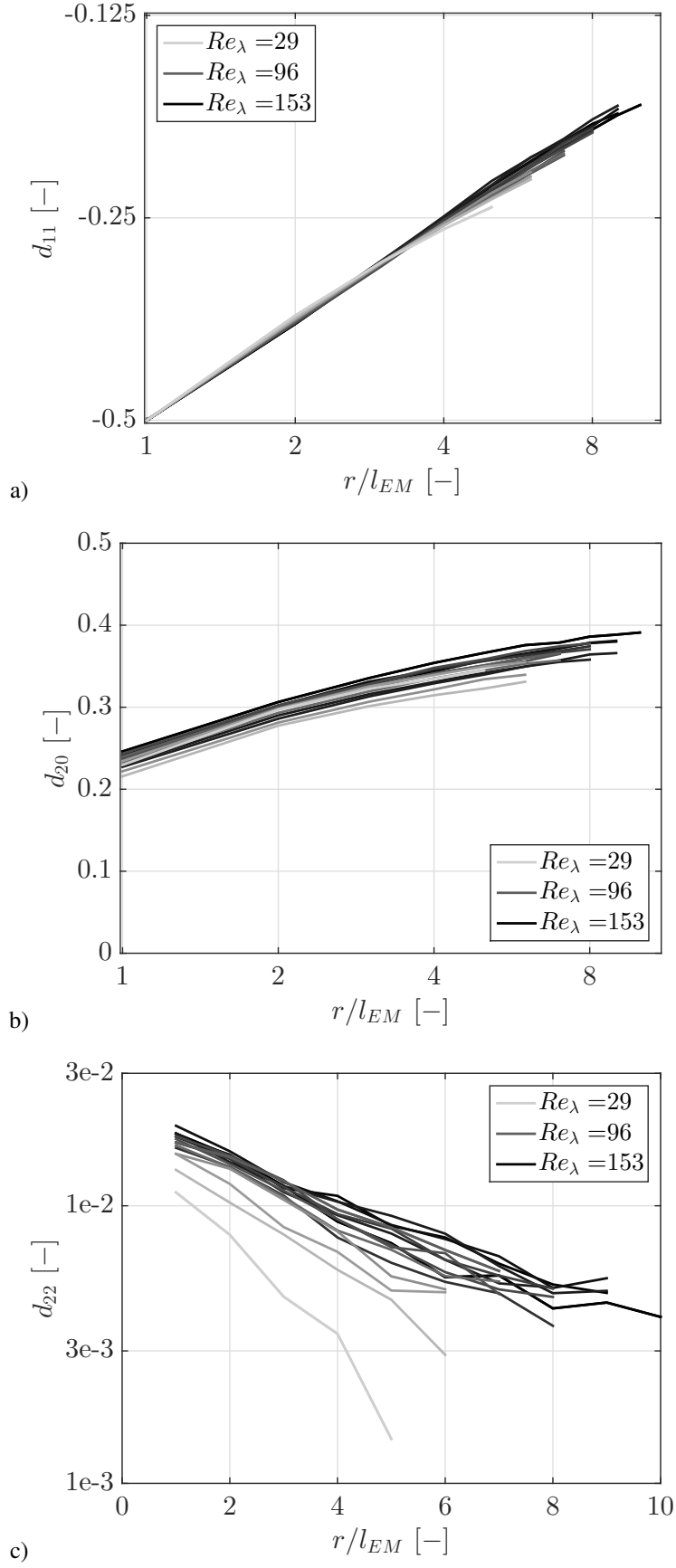


Figure 9: Parameters of grid generated turbulence as function of scale. The greyscale indicates Re_λ . a) shows d_{11} in a double-logarithmic plot. b) shows d_{20} in a semi-logarithmic plot. c) shows d_{22} in a semi-logarithmic plot

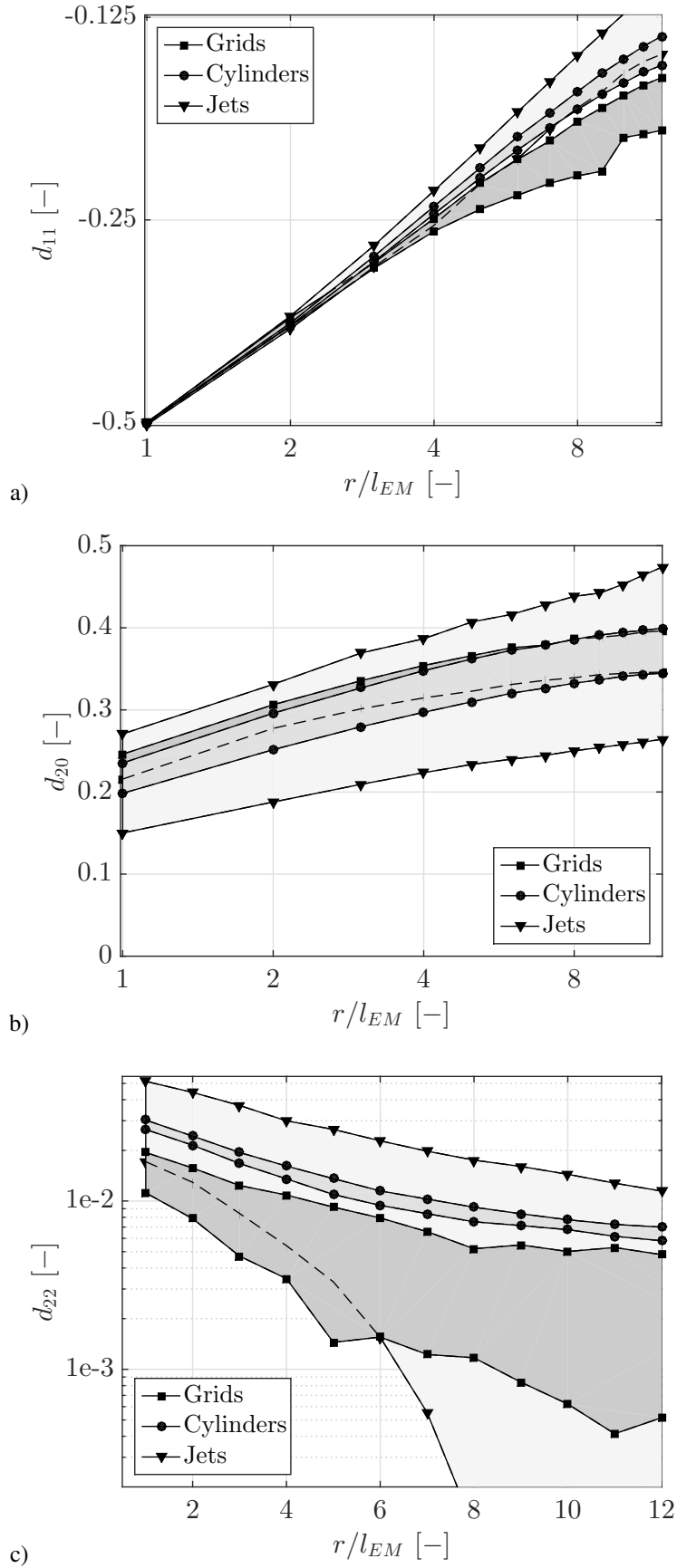


Figure 10: Parameters (d_{11} , d_{20} and d_{22}) as function of scale. Surfaces indicate areas where the parameters of specific turbulent flow are located. a) shows d_{11} in a double-logarithmic plot. b) shows d_{20} in a semi-logarithmic plot. c) shows d_{22} in a semi-logarithmic plot

edges are overlaid.

At small scales all d_{11} converge to an approximately linear functional form with the value of 0.5 at $r = l_{EM}$, as shown in figure 10 a). Therefore, universal scaling features of d_{11} are found for our datasets at small scales. This is confirmed by plotting the Reynolds number dependence of $d_{11}(r = l_{EM})$, see fig. 11 a). At larger scales we see that three groups are differently broad in the bending regime. To characterise this behavior the values of $d_{11}(r = 4l_{EM})$ as a function of Re_λ are shown in fig. 11 b). This indicates that the different behavior in d_{11} is mainly a Reynolds number effect and does not show significant differences for the different flows. Thus, the analysis of d_{11} shows an uniform picture of the different turbulent flows. At small scales d_{11} gets a universal form, which shows no dependency on the kind of turbulent flow, neither on Re_λ . At larger scales Re_λ becomes important, but the kind of flow does not have a strong effect on d_{11} features.

Figure 10 b) shows d_{20} . The three groups of flows increase with scale in a similar manner. As a further characterisation we show the Reynolds number dependence of d_{20} again for two selected scale $r = l_{EM}$ and $r = 4l_{EM}$ in figs. 11 c) and d). The overall trend of the entire datasets is rather constant, thus a quite uniform band of data is obtained. Note, d_{20} is sensitive on the normalisation of the velocity increment series, eq. (7). The norm σ_Θ leads to this weak dependency of d_{20} on Re_λ . In contrast $\sigma_\infty = \sqrt{2}\sigma(v)$ as norm leads to a distinct dependency of d_{20} on Re_λ , what supports our procedure to use the new values of Θ and σ_Θ for normalisation. The values start to scatter more beyond $Re_\lambda > 200$. Even one jet dataset is increasing whereas the others are decreasing. Thus, we conclude that to a good approximation all d_{20} show a similar behavior, which depends in a rather unsystematically way on Re_λ and not on the type of the flow.

Figure 10 c) shows d_{22} . The turbulent flows show in d_{22} distinct groups. These groups are different in shape and broadness. Whereby, from bottom to top the functional form of the group's borders changes in a quite systematical way. To investigate whether this behavior can be explained by a Re_λ -dependency or not we proceed as above by plotting $d_{22}(r = l_{EM})$ and $d_{22}(r = 4l_{EM})$ as a function of Re_λ , see figs. 11 e) and f). In contrast to the findings of d_{11} and d_{20} now the data does not collapse on a uniform Re_λ behavior, but clearly disjunct dependencies can be see. Each dataset seems to follow a different evolution with Re_λ . Most interestingly, this also holds for the case of small scales $r = l_{EM}$, for which a convergence to a flow type independent behavior should be expected in the common understanding of turbulence.

We further extend our research and try to combine the various subgroups of d_{22} . d_{22} as function of the dimensionless length $\frac{L}{\lambda}$ indicates the possibility of combining subgroups of one flow type. However, the different flow types can not be combined to one universal evolution, see appendix A7.

5 Conclusion

Finally we discuss our findings in the context of the common understanding of turbulence, in which large scale structures, where energy is feed into a cascade process, are known to be dependent on the generating process. It is commonly believed that small scale structures have flow independent features. This assumption of universal small scale structures is utilized in turbulence modeling. To which degree such a universal behavior is present, will be discussed next on the background of our results on structure functions and multi-scale statistics.

The analysis of the flow datasets shows at first glance the common scaling picture of homogenous isotropic turbulence in terms of structure function features (2-point statistics, cf. Kolmogorov (1962)), although various different flows are compared. Closer investigation of local scaling exponents, grasping the deviations from proper scaling features, can be set in a common dependency on Re_λ . This deviation feature gets confirmed by results of Mydlarski and Warhaft (1996). Scattering of the shown results forbid to distinguish between different turbulent flows and no significant clustering is observed in regard to the generation of turbulence. Compared to other studies the observed scattering in our results is not unusual, cf. Gylfason and Warhaft (2004).

For this traditional analysis of the data by structure functions we introduced two new quantities Θ and σ_Θ for the purpose of normalisation. As these quantities are dimensional and contain information of the large scale structures, we find pronounced clustering with respect to the considered turbulent flows.

For all 61 different datasets we could show the validity of the IFT. Therefore, we propose that the IFT can be taken as a new general thermodynamical law for the turbulent cascade. It is the IFT in combination with a self consistent optimisation procedure, which enables to work out significant contributions to the stochastic cascade process. For all data, we see that the cascade process is given by three aspects and parameters. A deterministic part, expressed by d_{11} , that corresponds to a returning force which pulls increments with decreasing scales to the equilibrium state, thus describes the reduction of the magnitude of the increments with decreasing scales. The driving force is represented by an additive and a multiplicative noise term, given by d_{20} and d_{22} , that describe features of fluctuations around the deterministic evolution in the cascade process. The derived stochastic cascade model (based on these three parameters) leads to a closed sets of differential equations for structure functions, which allows a decent reproduction of structure functions, and includes correct deviations from proper scaling behavior (Kolmogorov, 1962).

The non-stationary stochastic cascade process of turbulence is represented by scale dependent parameters d_{ij} . Therefore, the aspects of universality can be investigated in detail. Our main finding is the evolution in scale of d_{11} as well as d_{20} are found to be universal in the sense that their are flow independent. Thus, their functional forms can be expressed by scale and Re_λ dependencies.

In strong contrast to the findings for the structure functions and findings of the parameters d_{11} and d_{20} , the features of the

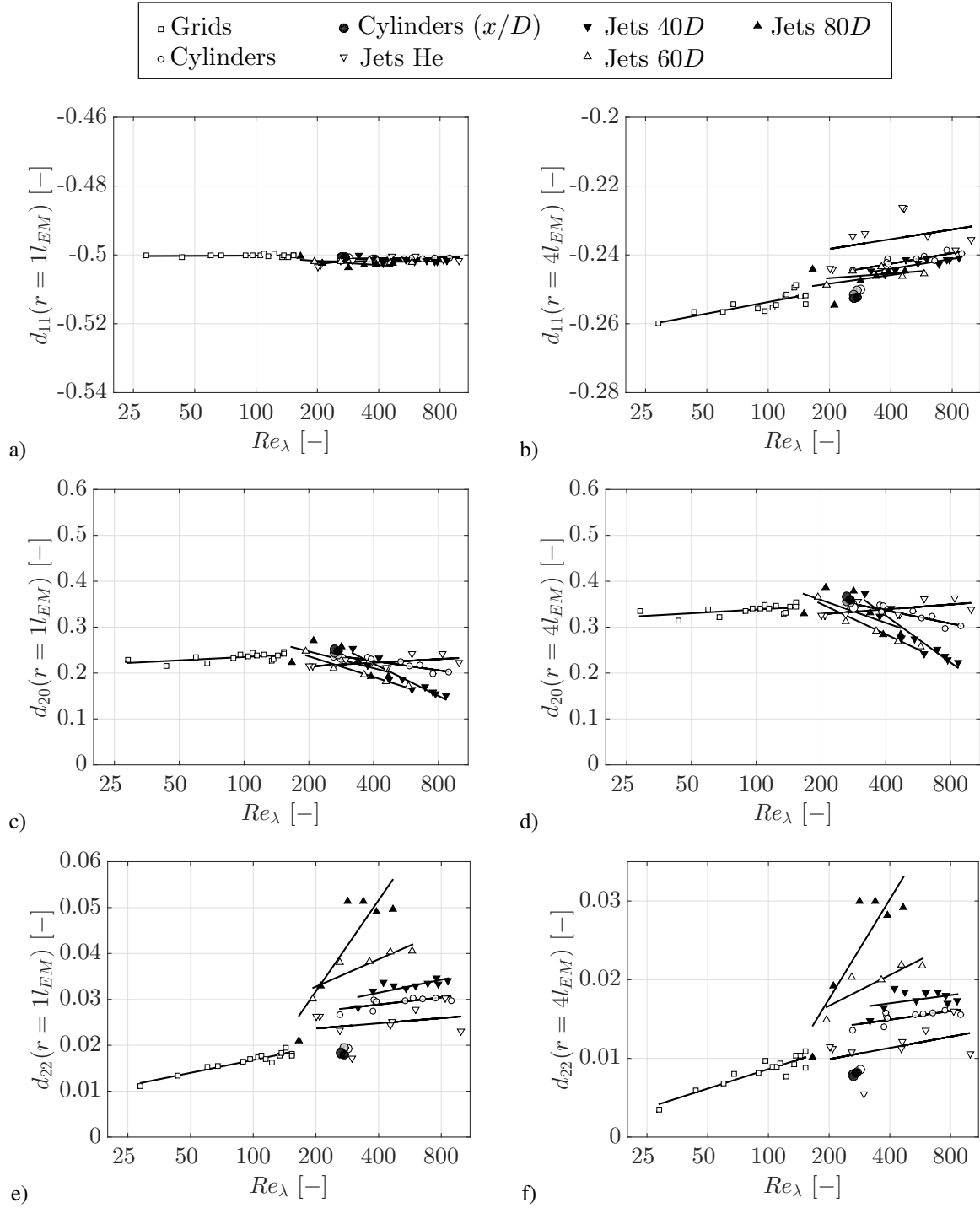


Figure 11: Parameters as function of Re_λ at two fixed scales ($r = l_{EM}$ and $4l_{EM}$). Additionally, *linear fit functions* indicate trends. All plots are semi-logarithmic plotted

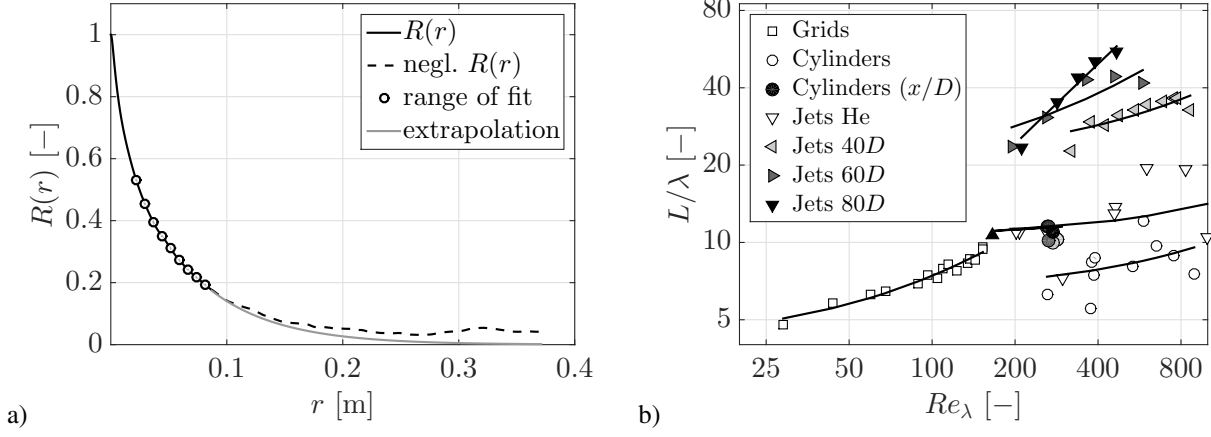


Figure 12: a) Illustration of the procedure of determining the integral length. Shown is the autocorrelation function, the considered part, solid black line and the neglected part, dashed black line, the range of fit, open circles and the extrapolation of $R(r)$, grey solid line. b) The $length$ of the inertial range $\frac{L}{\lambda}$ as function of Re_λ for all datasets.

intermittency causing parameter d_{22} as function of Re_λ split up in disjunct clusters for every considered dataset subgroup, characterized by specific large scale flow structures or the turbulence generation mechanism. We conclude that specific turbulent flows have their own particular multi-scale cascade, with other words their own stochastic fingerprint.

We like to acknowledge the funding from DFG and the cooperations as well as discussions with D. Bastine, A. Engel, A. Fuchs, A. Hadjihosseini, P. Lind, P. Milan, R. Stresing, M. R. R. Tabar and M. Wächter as well as for the experimental datasets provided by O. Chanal, St. Lück and Ch. Renner.

6 Appendix

A1: Determination of integral length

The determination of the integral length is based on the definition in Batchelor (1953, p. 47), where the autocorrelation $R(r)$ is integrated from zero to infinity. From a particle point of view the integration is stopped before infinite, thus, an upper limit r_{up} is needed. For our data we investigate, going from zero to larger scales, if the autocorrelation decreases monotonically with $\partial_r R(r) \leq 0$ and $\partial_{rr} R(r) \geq 0$. For this case the integration is done up to $R(r) \leq 0.01$. If this is not the case an r_{up} is defined by the location where the monotonous decrease is violated. From r_{up} on the autocorrelation function becomes extrapolated as inspired by Batchelor (1953, pp. 92-96, fig. 5.2),

$$L = \int_0^{r_{up}} R(r) dr + \frac{e^{a \cdot r_{up} + b}}{a}. \quad (31)$$

The parameters a and b are obtained by a fit routine. The fitting range is between r_{low} and r_{up} . Low border is chosen as the larger value of $r_{low} \rightarrow R(r_{low}) = \frac{2}{e}$ or $3R(r_{up})$. Figure 12 a) illustrates exemplary this procedure. Figure 12 b) shows the integral length L in units of the Taylor microscale λ over the Taylor based Reynolds number. For all subgroups of datasets the ratio $\frac{L}{\lambda}$ increases with Re_λ , as highlighted by *linear* fits. $\frac{L}{\lambda} \propto Re_\lambda$ can be derived from $L \approx \text{constant}$, $\lambda \propto Re^{-\frac{1}{2}}$ and $Re_\lambda \propto Re^{\frac{1}{2}}$ cf. Lück et al. (2006). Note, in figure 12 b) a double logarithmic presentation is used for reasons of clarity.

A2: Einstein-Markov coherence length

The Einstein-Markov coherence length l_{EM} is a length at which

$$p(u_r | u_{r+l_\Delta}) = p(u_r | u_{r+l_\Delta}, u_{r+2l_\Delta} = 0 \pm \chi), \quad (32)$$

$$\chi = 0.1\sigma_v, \quad (33)$$

is fulfilled. Lück et al. (2006) used the Wilcoxon test to verify this length, which can be considered as a *linear measure*. Here a test is used which is based on eq. (18). Since eq. (18) is a logarithmical measure, rare events are more strongly weighted. Figure 13 shows an exemplary examination of eq. (32) under variation of Δ , which is given in units of λ . The first steep part of ε is extrapolate to estimate l_{EM} . A first order polynomial ($O = 1$) leads to a similar result as published by

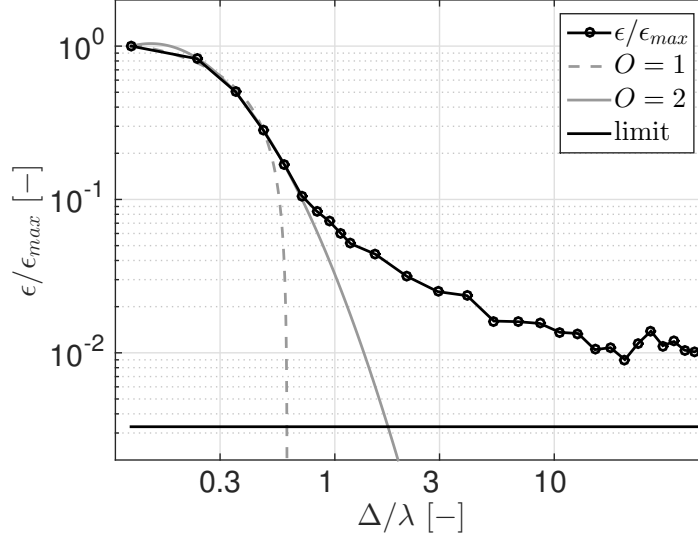


Figure 13: Test of the Markov property by normalised ε , according to eq. (18), with PDFs from the left and right hand side of eq. (32). The limit indicates the best expected ε . Fits of first and second order estimates l_{EM}

Type	Re_λ	α_{11}	β_{11}	$100\alpha_{22}$	$100\beta_{22}$	$100\alpha_{20}$	$100\beta_{20}$
grid	28	3.85	-0.29	-0.47	0.93	2.19	1.15
grid (i)	153	3.97	-0.29	-0.56	1.68	2.27	1.34
free jet (i)	166	4.19	-0.91	-0.85	2.2	2.16	0.98

Table 3: d_{ij} parameterisation in terms of α_{ij} and β_{ij} , see also table 1

Lück et al. (2006) and a second order polynomial ($O = 2$) leads to a higher estimation of $l_{EM} \approx 2\lambda$. For both estimations ($O = 1$ and $O = 2$) of l_{EM} a non-Markovian share remain. Note, the relation between l_{EM} and λ slightly changes the IFT convergence, $l_{EM} = \lambda \rightarrow \langle I_{max} \rangle \approx 1.02$ and $l_{EM} = 2\lambda \rightarrow \langle I_{max} \rangle \approx 1.01$.

A3: Characterisation of norms

Figure 14 shows the dimensional norms Θ and σ_Θ as function of Re_λ . Θ is plotted in a double logarithmic fashion, thereby a power law dependency from Re_λ becomes evident. σ_Θ depends linearly on Re_λ , figure 14 b). For both quantities the different generated flows show up in individual clusters, which are interestingly arranged in different ways. Although, Θ and σ_Θ are connected by their definition, the different arrangement and the different functional dependency from Re_λ show that their are not trivial linked to each other. The ratio $\frac{\Theta}{\lambda}$ (e.g. as function of Re_λ) shows a rather scattered distribution, values are between 2 and ~ 4 , however, some ratios go up to ~ 7 .

A4: Structure functions deduced by $D^{(1,2)}$

Eq. (27) allows to calculate the structure functions and $\xi_\kappa(r)$ from the parameters d_{ij} . Figure 15 shows our approaches of a proper parameterisations according to $d_{11} = (\alpha_{11} \frac{r}{l_{EM}} + \beta_{11})^{-\frac{1}{2}}$, $d_{22} = \alpha_{22} \ln(\frac{r}{l_{EM}}) + \beta_{22}$ and $d_{20} = (\alpha_{20} \ln(\frac{r}{l_{EM}}) + \beta_{20})^{\frac{1}{3}}$. For this illustration three different datasets are used. The Re_λ -values and the corresponding fit parameters α_{ij} and β_{ij} as well as the flow type are summarised in table 3.

The local scaling exponents are shown in figure 16, which are deduced directly from the velocity increments and from the parameters using eq. (27). The values of the optimised $D^{(1,2)}$ as well as the mentioned fit functions of parameters d_{ij} are used. Here - as an exception - with $l_{EM} = \lambda$ to highlight the crossing of K62. Note, the *jumpy development* of ξ_κ is caused by a linear interpolation of $D^{(1,2)}$. An error margin of $\xi_\kappa(r)$ was derived from the experimental data. This is done by splitting the measured data in n -groups and determining n -time $\xi_\kappa(r)$, from which the standard deviation $\sigma(\xi_\kappa^n(r))$ is calculated. In this way ($n = 50$)

$$\Delta \xi_\kappa(r) = \frac{\sigma(\xi_\kappa^n(r))}{\sqrt{n}}, \quad (34)$$

is determined. As an orientation also Kolmogorovs prediction according to eq. (5) is shown (labeled K62), likewise to figure 2 a).

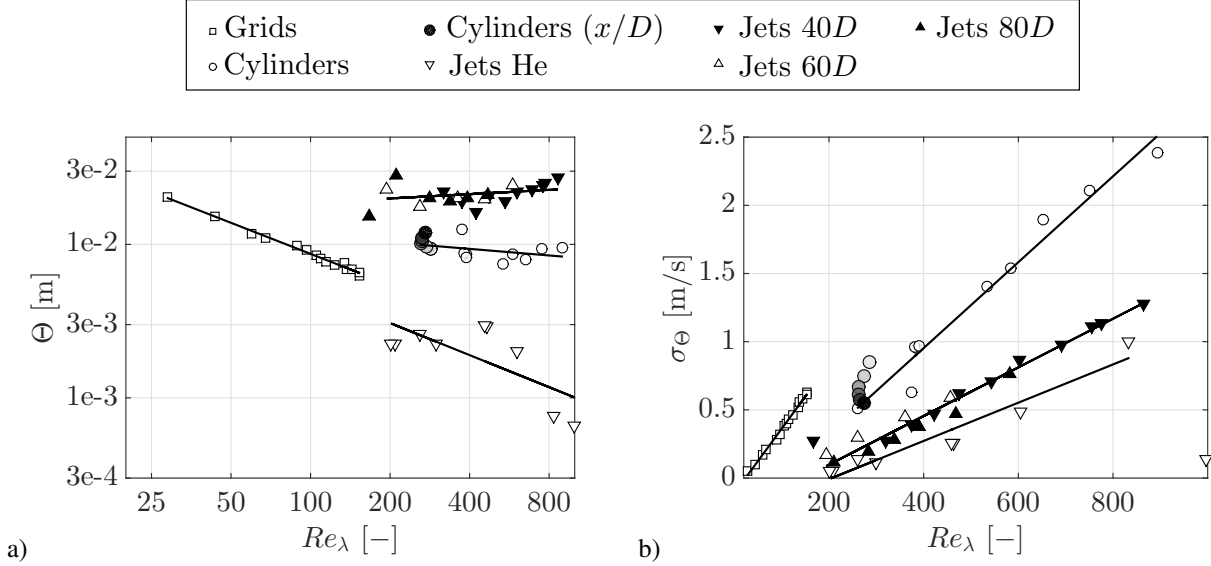


Figure 14: a) shows the norm Θ over Re_λ in a double logarithmic plot. b) shows the norm σ_Θ over Re_λ . Both norms are shown for all datasets. Trends are highlighted by linear fit functions

A5: Interpretation of $D^{(1)}$ and $D^{(2)}$ with the short time propagator

The interpretation of $D^{(1,2)}$ and d_{11}, d_{22}, d_{20} is done by modifying optimised $D^{(1,2)}$ and presenting the corresponding short time propagator. The short time propagator deduced by unmodified d_{11}, d_{22} and d_{20} (regular optimised) is shown in figure 17 a). The agreement is good between short time propagator and the experimental reference data. In figure 17 b) d_{11} is multiplied by 5, whereas d_{22} and d_{20} are unmodified. This multiplication twists the diagonal of short time propagator in comparison to the experimental reference data. Thus, we see that the magnitude of d_{11} controls the diagonal. In figure 17 c) d_{22} is multiplied by 5, whereas d_{11} and d_{20} are unmodified. An enlarged d_{22} increases the curvature of the isolines in the contour plot. Therefore, the probability for extreme events increases, which is equivalent to an increased intermittency of unconditional PDFs. In figure 17 d) d_{20} is multiplied by 5, whereas d_{11} and d_{22} are unmodified. Here the reconstructed distribution gets broader around the distribution diagonal.

A6: Single developments of d_{11}, d_{22} and d_{20} in scale

For the sake of completeness, the coefficients d_{11}, d_{22} and d_{20} are shown for cylinder and free jet flows as function of scale in figures 18 - 20. These figures are just the same as figure 9.

A7: d_{22} as function of $\frac{L}{\lambda}$

Findings of figures 11 e) and f) can be further investigated in terms of universality by interpreting d_{22} as function of a different quantity. For instance, plotting d_{22} as function of the dimensionless length $\frac{L}{\lambda}$ (relative length of inertial range) the results become new sorted and gives a much more uniform picture, see figures 21 a) and b). Although, single free jet subgroups might be systematically distinguished in terms of the relative distance to the nozzle, the entire free jet datasets show a rather uniform group in contrast to figures 11 e) and f). The relative location of the *Cylinder* subgroup differs clearly from the other data in this presentation. Although d_{22} is more sorted, we come to the same conclusion as above, intermittency features in terms of d_{22} are non-universal, and single flow types become apparent.

References

- A. Arneodo, C. Baudet, F. Belin, R. Benzi, B. Castaing, B. Chabaud, R. Chavarria, S. Ciliberto, R. Camussi, F. Chillá, B. Dubrulle, Y. Gagne, B. Hebral, J. Herweijer, M. Marchand, J. Maurer, J. F. Muzy, A. Naert, A. Noullez, J. Peinke, F. Roux, P. Tabeling, W. van de Water, and H. Willaime. Structure functions in turbulence, in various flow configurations, at Reynolds number between 30 and 5000, using extended self-similarity. *EPL (Europhysics Letters)*, 34(6):411, 1996. URL <http://stacks.iop.org/0295-5075/34/i=6/a=411>.
- D. Aronson and L. Löfdahl. The plane wake of a cylinder: Measurements and inferences on turbulence modeling. *Physics of Fluids A*, 5:1433–1437, June 1993. doi: 10.1063/1.858579.
- G. K. Batchelor. *The theory of homogeneous turbulence*. Cambridge science classic, Cambridge, 1953.

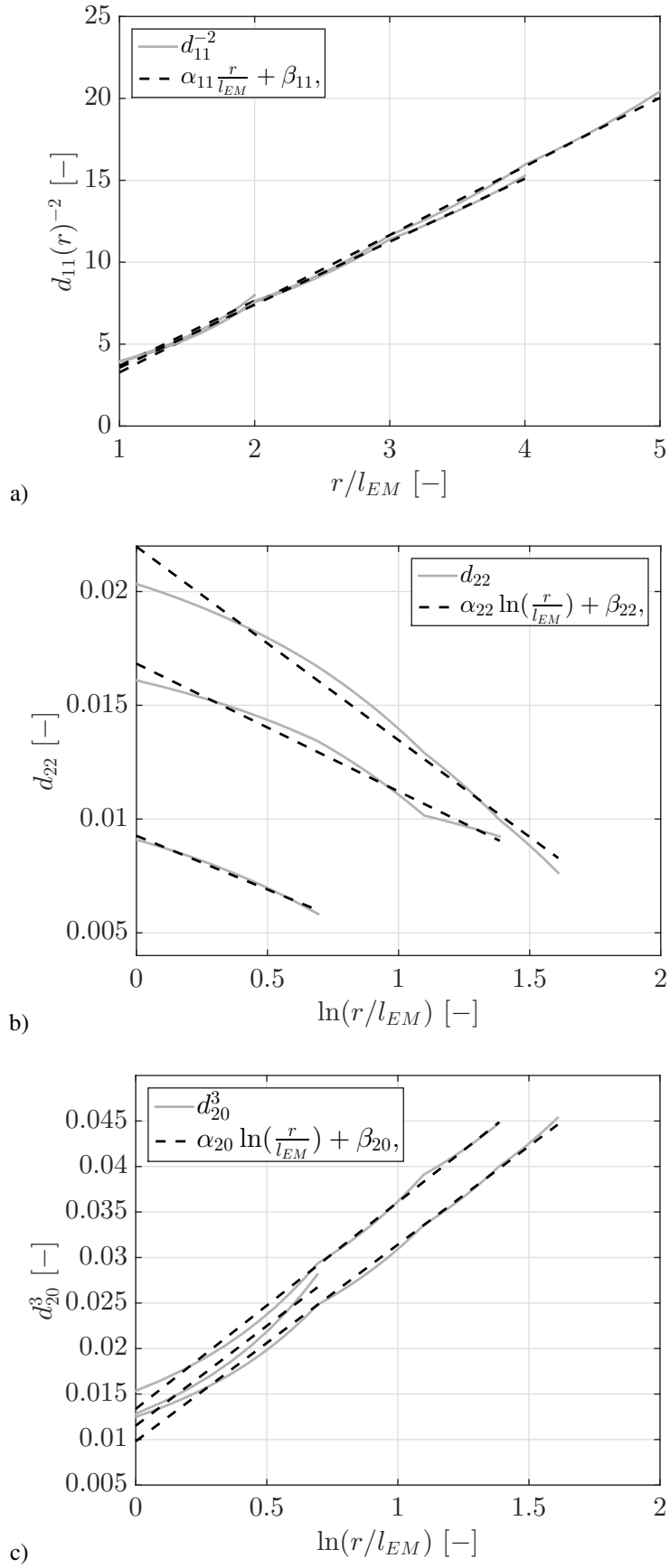


Figure 15: d_{ij} in a linearised form as well as fit functions. Length of d_{ij} corresponds to Re_λ , see table 3

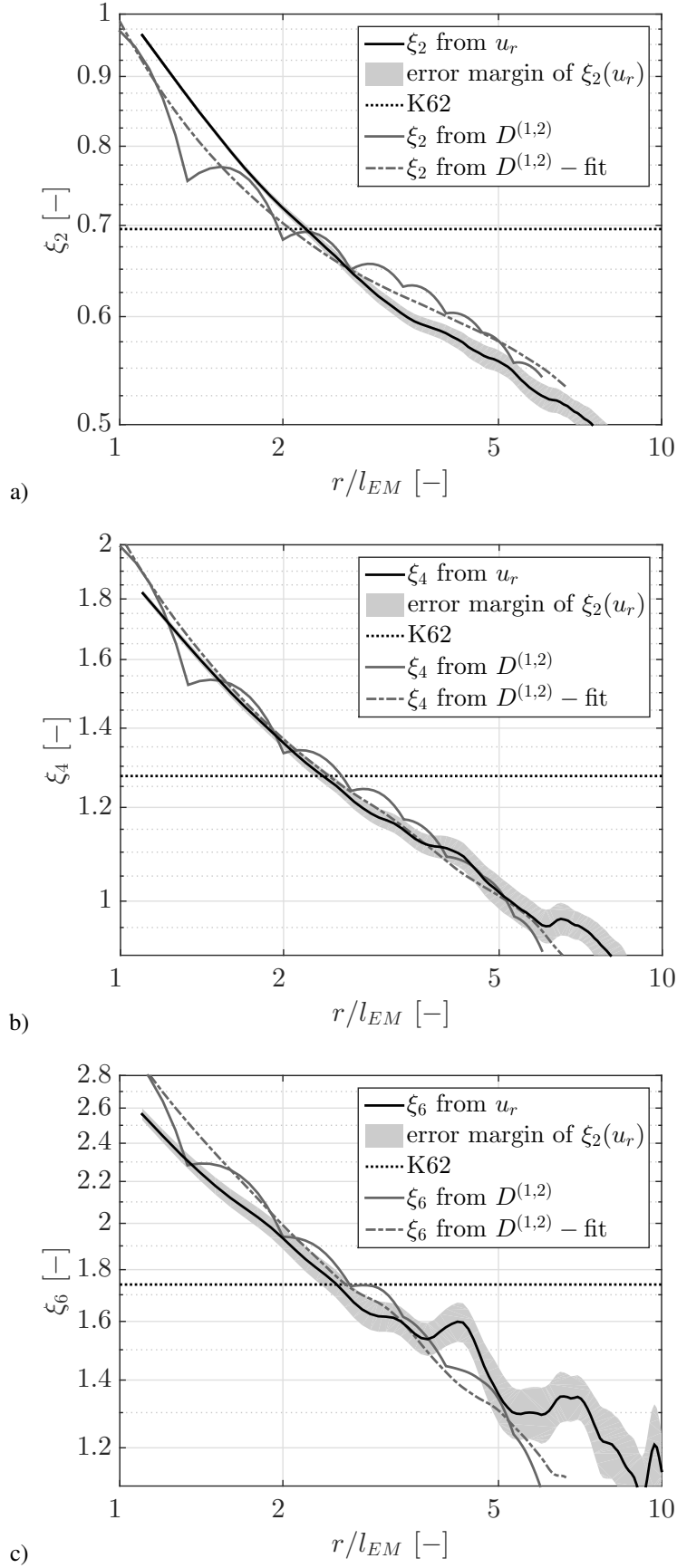


Figure 16: Local scaling exponent $\xi_\kappa(r)$ deduced from experimental data, reconstructed by $D^{(1,2)}$ as well as their fits. Also Kolmogorov's prediction is shown (K62) and an error margin of the experimental data. Grid (i) is used as exemplary dataset, characterised in table 1 and 3

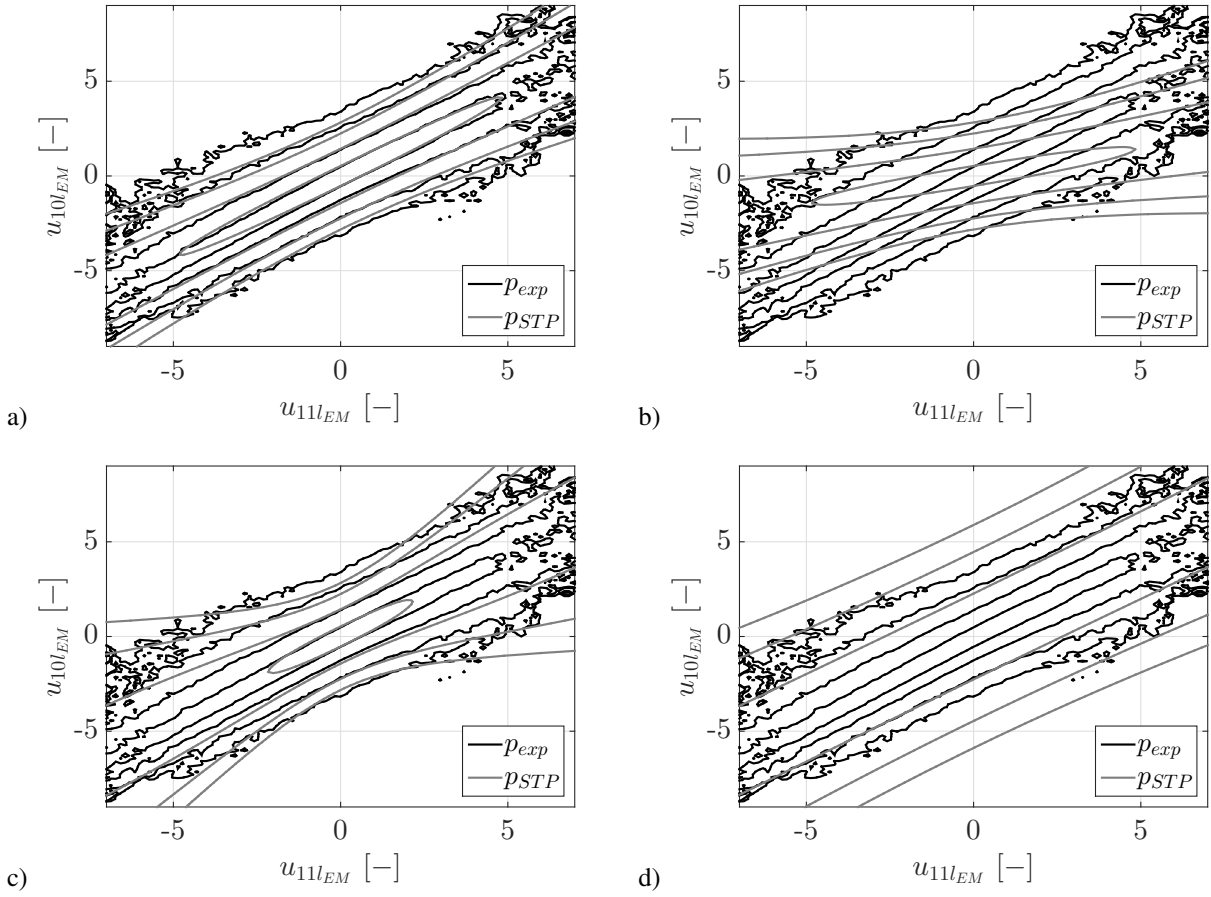


Figure 17: One exemplary experimentally found conditional PDF, p_{exp} (black) (subgroup (v), $Re_\lambda = 475$) and four different results of the short time propagator p_{STP} (grey). Figure a) shows the short time propagator result regarding to optimised $D^{(1,2)}$. In figure b) the same is shown as in a) except that d_{11} is multiplied by 5. In figure c) only d_{22} is multiplied by 5 and in figure d) only d_{20} is multiplied by 5

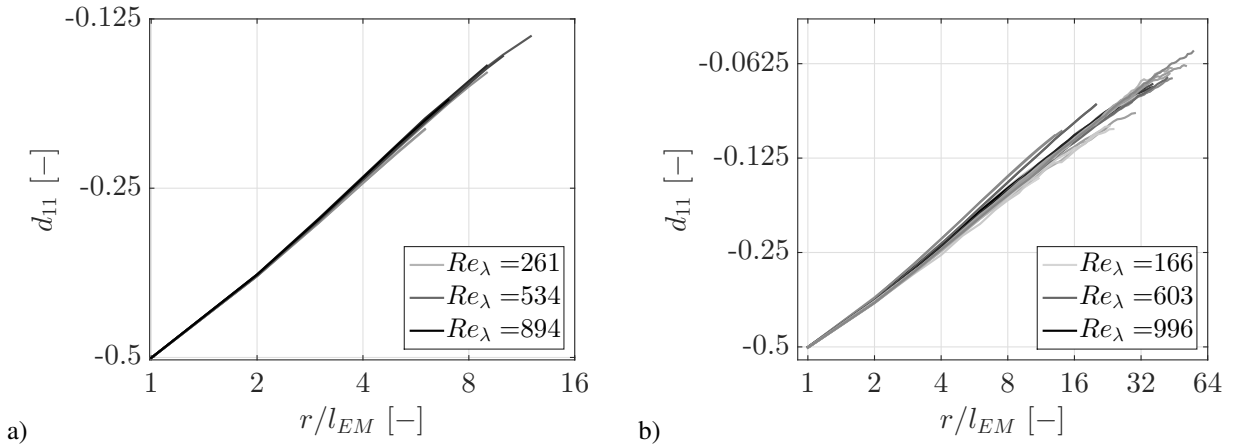


Figure 18: d_{11} as function of scale, of cylinder flows (a) and free jet flows (b). Lines greyscale indicates Re_λ

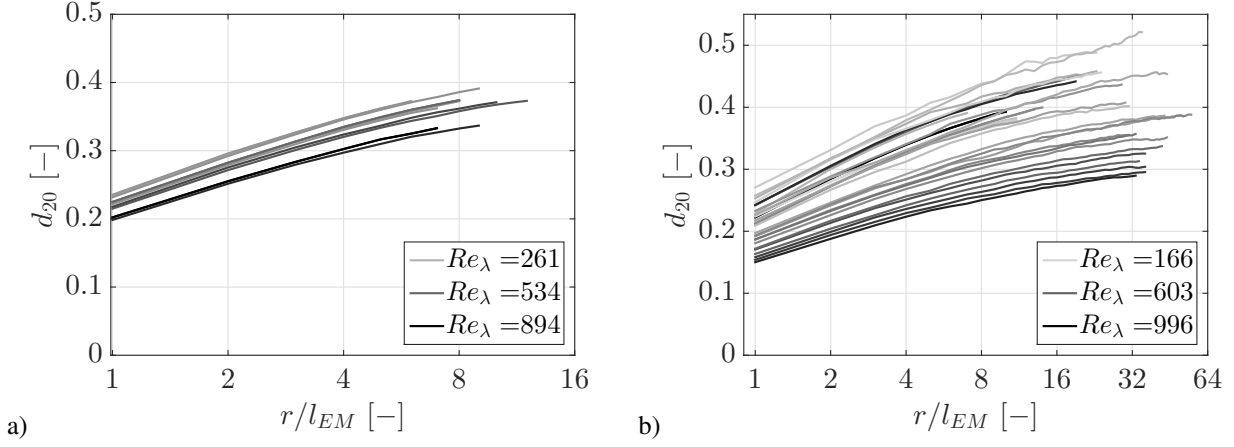


Figure 19: d_{20} as function of scale, of cylinder flows (a) and free jet flows (b). Lines greyscale indicates Re_λ

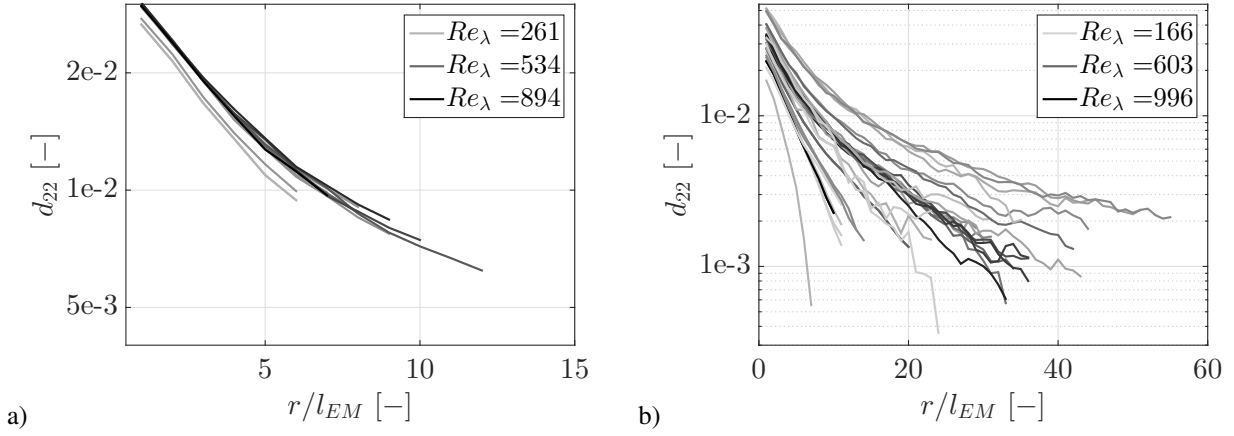


Figure 20: d_{22} as function of scale, of cylinder flows (a) and free jet flows (b). Lines greyscale indicates Re_λ

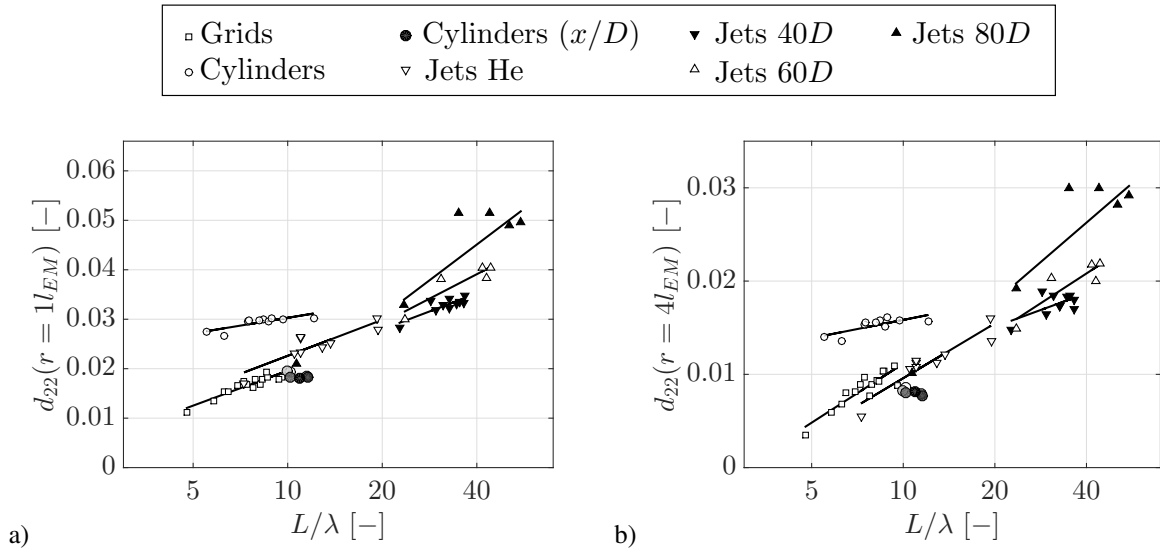


Figure 21: Parameter d_{22} as function of L/λ at two fixed scales ($r = l_{EM}$ and $4l_{EM}$). Additionally, *linear* fit functions indicate trends. Plots are semi-logarithmic plotted

- R. Friedrich Ch. Renner, J. Peinke. On the interaction between velocity increment and energy dissipation in the turbulent cascade. *Physics of Fluid Dynamics*, 2013.
- O. Chanal, B. Chabaud, B. Castaing, and B. Hébral. Intermittency in a turbulent low temperature gaseous helium jet. *The European Physical Journal B - Condensed Matter and Complex Systems*, 17(2):309–317, 2000. ISSN 1434-6028. doi: 10.1007/s100510070146. URL <http://dx.doi.org/10.1007/s100510070146>.
- Clay. *Millennium problems*. Clay Mathematics Institute: <http://www.claymath.org/millennium-problems>, 2000.
- P. A. Davidson. *Turbulence: an introduction for scientists and engineers*. Oxford University Press, USA, 2004.
- Jahanshah Davoudi and M. Reza Rahimi Tabar. Multiscale correlation functions in strong turbulence. *Physical Review E*, 61(6), 2000.
- A. Einstein. Über die von der molekularkinetischen theorie der wärme geforderte bewegung von in ruhenden flüssigkeiten suspendierten teilchen. *Annalen der Physik*, 322(8):549–560, 1905. ISSN 1521-3889. doi: 10.1002/andp.19053220806. URL <http://dx.doi.org/10.1002/andp.19053220806>.
- William Feller. *An Introduction to Probability Theory and Its Applications*, volume 1. Wiley, January 1968. ISBN 0471257087. URL <http://www.amazon.ca/exec/obidos/redirect?tag=citeulike04-20{&}path=ASIN/0471257087>.
- R. Friedrich and J. Peinke. Description of a turbulent cascade by a fokker-planck equation. *Phys. Rev. Lett.*, 78:863, 1997.
- U. Frisch. *Turbulence: the legacy of A. N. Kolmogorov*. Cambridge University Press, 2001.
- E. Gledzer. On the Taylor hypothesis corrections for measured energy spectra of turbulence. *Physica D Nonlinear Phenomena*, 104:163–183, February 1997. doi: 10.1016/S0167-2789(96)00300-4.
- Julia Gottschall and Joachim Peinke. On the definition and handling of different drift and diffusion estimates. *New Journal of Physics*, 10(8):083034, 2008. URL <http://stacks.iop.org/1367-2630/10/i=8/a=083034>.
- Rainer Grauer, Holger Homann, and Jean-Francois Pinton. Longitudinal and transverse structure functions in high-reynolds-number turbulence. *New Journal of Physics*, 14(6):063016, 2012. URL <http://stacks.iop.org/1367-2630/14/i=6/a=063016>.
- A. Gylfason and Z. Warhaft. On higher order passive scalar structure functions in grid turbulence. *Physics of Fluids*, 16: 4012–4019, November 2004. doi: 10.1063/1.1790472.
- Christoph Honisch and Rudolf Friedrich. Estimation of kramers-moyal coefficients at low sampling rates. *Phys. Rev. E*, 83:066701, Jun 2011. doi: 10.1103/PhysRevE.83.066701. URL <http://link.aps.org/doi/10.1103/PhysRevE.83.066701>.
- D. Hurst and J. C. Vassilicos. Scalings and decay of fractal-generated turbulence. *Physics of Fluids*, 19(3):035103, 2007. doi: <http://dx.doi.org/10.1063/1.2676448>. URL <http://scitation.aip.org/content/aip/journal/pof2/19/3/10.1063/1.2676448>.
- C. Jarzynski. Nonequilibrium equality for free energy differences. *Phys. Rev. Lett.*, 78:2690–2693, Apr 1997. doi: 10.1103/PhysRevLett.78.2690. URL <http://link.aps.org/doi/10.1103/PhysRevLett.78.2690>.
- C. J. Keylock, R. Stresing, and J. Peinke. Gradual wavelet reconstruction of the velocity increments for turbulent wakes. *Physics of Fluids*, 27(2):025104, 2015. doi: <http://dx.doi.org/10.1063/1.4907740>. URL <http://scitation.aip.org/content/aip/journal/pof2/27/2/10.1063/1.4907740>.
- D. Kleinhans, R. Friedrich, A. P. Nawroth, and J. Peinke. An iterative procedure for the estimation of drift and diffusion coefficients of langevin processes. *Phys. Letters A*, 346:42–46, 2005.
- A. N. Kolmogorov. Dissipation of energy in locally isotropic turbulence. In *Dokl. Akad. SSSR*, volume 32, pages 16–18, 1941.
- A. N. Kolmogorov. A refinement of previous hypotheses concerning the local structure of turbulence in a viscous incompressible fluid at high reynolds number. *Journal of Fluid Mechanics*, 13:82–85, 5 1962. ISSN 1469-7645. doi: 10.1017/S0022112062000518. URL http://journals.cambridge.org/article_S0022112062000518.
- Arkadiusz K. Kuczaj, Bernard J. Geurts, and W. David McComb. Nonlocal modulation of the energy cascade in broadband-forced turbulence. *Phys. Rev. E*, 74:016306, Jul 2006. doi: 10.1103/PhysRevE.74.016306. URL <http://link.aps.org/doi/10.1103/PhysRevE.74.016306>.

- C. C. Lin. On Taylor's hypothesis in wind tunnel turbulence. *Memor. U.S. Naval Ord. Lab. no. 10775*, 1950.
- St. Lück, Ch. Renner, J. Peinke, and R. Friedrich. The markov-einstein coherence length - a new meaning for the Taylor length in turbulence. *Physics Letters A*, 359(5):335–338, 2006. ISSN 0375-9601. doi: <http://dx.doi.org/10.1016/j.physleta.2006.06.053>. URL <http://www.sciencedirect.com/science/article/pii/S0375960106009728>.
- J. L. Lumley. Interpretation of time spectra measured in high intensity shear flows. *Physics of Fluids*, 8(6):1056–1062, 1965. doi: <http://dx.doi.org/10.1063/1.1761355>. URL <http://scitation.aip.org/content/aip/journal/pof1/8/6/10.1063/1.1761355>.
- T. S. Lundgren. Distribution functions in the statistical theory of turbulence. *Physics of Fluids*, 10(5):969–975, 1967. doi: <http://dx.doi.org/10.1063/1.1762249>. URL <http://scitation.aip.org/content/aip/journal/pof1/10/5/10.1063/1.1762249>.
- Victor L'vov and Itamar Procaccia. Fusion rules in turbulent systems with flux equilibrium. *Phys. Rev. Lett.*, 76:2898–2901, Apr 1996. doi: 10.1103/PhysRevLett.76.2898. URL <http://link.aps.org/doi/10.1103/PhysRevLett.76.2898>.
- Matthew S. Melius, Murat Tutkun, and Raúl Bayoán Cal. Identification of markov process within a wind turbine array boundary layer. *Journal of Renewable and Sustainable Energy*, 6(2):023121, 2014. doi: <http://dx.doi.org/10.1063/1.4869566>. URL <http://scitation.aip.org/content/aip/journal/jrse/6/2/10.1063/1.4869566>.
- Andre Sergeevich Monin, AM IAglom, and John Leask Lumley. *Statistical fluid mechanics: mechanics of turbulence*, volume 1. Courier Corporation, 2007.
- A.S. Monin. Equations of turbulent motion. *Journal of Applied Mathematics and Mechanics*, 31(6):1057 – 1068, 1967. ISSN 0021-8928. doi: [http://dx.doi.org/10.1016/0021-8928\(67\)90210-9](http://dx.doi.org/10.1016/0021-8928(67)90210-9). URL <http://www.sciencedirect.com/science/article/pii/0021892867902109>.
- Frédéric Murzyn and Michel Bêlorgey. Experimental investigation of the grid-generated turbulence features in a free surface flow. *Experimental Thermal and Fluid Science*, 29(8):925 – 935, 2005. ISSN 0894-1777. doi: <http://dx.doi.org/10.1016/j.expthermflusci.2005.02.002>. URL <http://www.sciencedirect.com/science/article/pii/S0894177705000117>.
- L. Mydlarski and Z. Warhaft. On the onset of high-reynolds-number grid-generated wind tunnel turbulence. *Journal of Fluid Mechanics*, 320:331–368, 8 1996. ISSN 1469-7645. doi: 10.1017/S0022112096007562. URL http://journals.cambridge.org/article_S0022112096007562.
- Kouji Nagata, Yasuhiko Sakai, Takuto Inaba, Hiroki Suzuki, Osamu Terashima, and Hiroyuki Suzuki. Turbulence structure and turbulence kinetic energy transport in multiscale/fractal-generated turbulence. *Physics of Fluids*, 25(6):065102, 2013. doi: <http://dx.doi.org/10.1063/1.4811402>. URL <http://scitation.aip.org/content/aip/journal/pof2/25/6/10.1063/1.4811402>.
- A. P. Nawroth, J. Peinke, D. Kleinhans, and R. Friedrich. Improved estimation of fokker-planck equations through optimisation. *Phys. Rev. E.*, 76(056102), 2007.
- M. Nelkin. In What Sense Is Turbulence an Unsolved Problem? *Science*, January 1992. URL <http://www.sciencemag.org/cgi/content/abstract/255/5044/566>.
- Daniel Nickelsen and Andreas Engel. Probing small-scale intermittency with a fluctuation theorem. *Physical Review Letters*, 110:214501, May 2013. doi: 10.1103/PhysRevLett.110.214501.
- Pinton, J. F. and Labbé, R. Correction to the Taylor hypothesis in swirling flows. *J. Phys. II France*, 4(9):1461–1468, 1994. doi: 10.1051/jp2:1994211. URL <http://dx.doi.org/10.1051/jp2:1994211>.
- S. B. Pope. *Turbulent Flows*. Cambridge University Press, 2000. ISBN 9780521598866. URL <http://books.google.de/books?id=HZsTw9SMx-OC>.
- J. Zeller R. Friedrich and J. Peinke. A note on three-point statistics of velocity increments in turbulence. *Europhys. Lett.*, 41(2), 1998.
- N. Reinke, A. Fuchs, M. Hölling, and J. Peinke. Stochastic analysis of a fractal grid wake. *Progress in Turbulence VI, Proceedings of the iTi Conference on Turbulence 2014, Springer Proceedings in Physics*, 6, 2014.
- N. Reinke, D. Nickelsen, A. Engel, and J. Peinke. Application of an integral fluctuation theorem to turbulent flows. *Progress in Turbulence VI, Proceedings of the iTi Conference on Turbulence 2014, Springer Proceedings in Physics*, 165:19 – 25, 2016.

- C. Renner. Markowanalysen stochastisch fluktuierender zeitreihen. *Dissertation*, January 2002.
- C. Renner, J. Peinke, and R. Friedrich. Experimental indications for markov properties of small-scale turbulence. *J. Fluid Mech.*, 433:383–409, 2001.
- C. Renner, J. Peinke, R. Friedrich, O. Chanal, and B. Chabaud. Universality of small scale turbulence. *Phys. Rev. Lett.*, 89:124502, Sep 2002. doi: 10.1103/PhysRevLett.89.124502. URL <http://link.aps.org/doi/10.1103/PhysRevLett.89.124502>.
- L. F. Richardson. *Weather prediction by numerical process*. Cambridge University Press, 1922.
- H. Risken. *The Fokker-Planck Equation*. Springer, Heidelberg, 1984.
- U. Seifert. Entropy Production along a Stochastic Trajectory and an Integral Fluctuation Theorem. *Physical Review Letters*, 95(4):040602, July 2005. doi: 10.1103/PhysRevLett.95.040602.
- M. Sinhuber. On the scales of turbulent motion at high reynolds numbers. *Dissertation*, 2015.
- R. Stresing and J. Peinke. Towards a stochastic multi-point description of turbulence. *New Journal of Physics*, 12(10):103046, 2010. URL <http://stacks.iop.org/1367-2630/12/i=10/a=103046>.
- R. Stresing, J. Peinke, R. E. Seoud, and J. C. Vassilicos. Defining a new class of turbulent flows. *Phys. Rev. Lett.*, 104:194501, May 2010. doi: 10.1103/PhysRevLett.104.194501. URL <http://link.aps.org/doi/10.1103/PhysRevLett.104.194501>.
- R. Stresing, D. Kleinhans, R. Friedrich, and J. Peinke. Publisher’s note: Different methods to estimate the einstein-markov coherence length in turbulence [phys. rev. e **83**, 046319 (2011)]. *Phys. Rev. E*, 85:029907, Feb 2012. doi: 10.1103/PhysRevE.85.029907. URL <http://link.aps.org/doi/10.1103/PhysRevE.85.029907>.
- G. I. Taylor. The spectrum of turbulence. *Proceedings of the Royal Society of London A: Mathematical, Physical and Engineering Sciences*, 164(919):476–490, 1938. ISSN 0080-4630. doi: 10.1098/rspa.1938.0032.
- Chenning Tong and Z. Warhaft. Passive scalar dispersion and mixing in a turbulent jet. *Journal of Fluid Mechanics*, 292:1–38, 6 1995. ISSN 1469-7645. doi: 10.1017/S0022112095001418. URL http://journals.cambridge.org/article_S0022112095001418.
- M. Tutkun and L. Mydlarski. Markovian properties of passive scalar increments in grid-generated turbulence. *New Journal of Physics*, 6(1):49, 2004. URL <http://stacks.iop.org/1367-2630/6/i=1/a=049>.
- P. C. Valente and J. C. Vassilicos. Universal dissipation scaling for nonequilibrium turbulence. *Phys. Rev. Lett.*, 108:214503, May 2012. doi: 10.1103/PhysRevLett.108.214503. URL <http://link.aps.org/doi/10.1103/PhysRevLett.108.214503>.